EXPERIMENTAL AND NUMERICAL INVESTIGATIONS OF CO-FLOW JET FLOW CONTROL AIRFOIL ENERGY EXPENDITURE

Michele Di Fronzo
Politecnico di Bari,
Corso di laurea specialistica in Ingegneria Meccanica
curriculum: Costruzioni Meccaniche e sperimentazioni
michele_233@hotmail.com

November 22, 2011

POLITECNICO DI BARI- UNIVERSITY OF MIAMI

EXPERIMENTAL AND NUMERICAL INVESTIGATIONS OF CO-FLOW JET
FLOW CONTROL AIRFOIL ENERGY EXPENDITURE

By

Michele DiFronzo

A THESIS

Submitted to the Faculty
of the Politecnico di Bari
connected to an internship
carried out at the University of Miami

Coral Gables, Florida

December 2011

POLITECNICO DI BARI-UNIVERSITY OF MIAMI

A THESIS

Submitted to the Faculty
of the Politecnico di Bari
connected to an internship
carried out at the University of Miami

EXPERIMENTAL AND NUMERICAL INVESTIGATIONS OF CO-FLOW JET
FLOW CONTROL AIRFOIL ENERGY EXPENDITURE

Michele DiFronzo

Approved:

_____
Gecheng Zha, Ph.D.
Associate Professor of

Mechanical & Aerospace Engineering

_____
Prof. Ing Giuseppe Pascazio
Professor of Computational Fluid dynam-
ics at Politecnico di Bari

Abstract

The work of thesis is related to an internship carried out by Michele Di Fronzo at University of Miami at Mechanical and aerospace department

EXCELLENT AIRCRAFT PERFORMANCE both in MILITARY and in COM-MERCIAL sector are going to be achieved by reducing the weight and the fuel consumption thanks to the revolutionary flow-control techniques. A co-flow jet (CFJ) airfoil NACA6415 with zero-net mass flux has been developed by ZHA et all [1–9]. The advantages introduced by the CFJ are basically: lift and stall AoA augmentation and drag reduction. A commercial aircraft that uses CFJ can reduce is fuel consumption of about 10%. The calculation of the Power consumption and in particular of the Power Coefficient of the CFJ system and the way in which it is affected from other parameters is the principal topic of this thesis. Numerical analysis and experimental testing were conducted on baseline and co-flow jet airfoils of the same plan form. The CFJ mechanism employs high pressure air injected along the span at the leading edge while a low pressure source removes the same amount of air along the span at the trailing edge. Hence, the net mass flux of the system is zero energy loss is minimized. The jet produced along the upper surface of the airfoil mixes with and excites the free stream flow resulting in increased lift, augmented stall margin, and decreased drag. At certain angles of attack the decreased drag is negative and thrust is produced. The research was comprised of different phases including computational fluid dynamics (CFD) simulations and wind tunnel testing. A computational fluid dynamics code, developed at the University of Miami, was used to study flow fields and to obtain analytical results of aerodynamic properties for the baseline and CFJ airfoils. A post processing code was developed for the calculation of the Power Coefficient. Modeling of both wing shapes utilized the baseline ordinates of a cambered NACA 6415 airfoil. The calculation of the Power Coefficient was conducted for a fixed Mach number of the free stream on three AoA:0°, 10° and 20° and Mach 0.04, 0.07, 0.1 were taken in consideration for the study cases.

Nomenclature

α	angle of attack of the wing
AoA	acronym that stands for Angle Of Attack
CFJ	Co-flow jet
P	power from the pump in
P_c	Power coefficient
C_L	lift coefficient
C_D	drag coefficient
L	Lift force
D	Drag force
$\mathbf{F}$	resultant force
$\mathbf{R}$	force from airfoil surface integral
$\mathbf{R'}$	reactionary force of $\mathbf{R}$
R_e	Reynolds number
M	Mach number
V	velocity
ρ	density
$\dot{m}$	mass flow rate
C_p	specific heat of the air by keeping constant pressure
γ	air specific heats ratio;suction coefficient: 1 suction ON, 2 suction OFF
θ	angle between slot surface and the line normal to the chord
R	elastic constant of ideal gas law
$1stPT$	first thermodynamic principle in eulerian and thermal form
P_0	air total pressure
T_0	air total temperature
$\Gamma = P_{01}/P_{02}$	
S	$S = spanXchord$ is the planform area of the wing
c	wing chord
h	slot's height
∞	subscript for the free stream values
$1, 2, 3$	subscripts for the mach numbers 0.04,0.07 and 0.1
inj, suc	subscripts for the injection and suction values
e	subscript for the control volume exit;

Acknowledgment

Contents

List of Figures

List of Tables

Chapter 1

Sommario in lingua italiana

La presente tesi e' il risultato finale di un intership da me svolto presso la University of Miami, nel dipartimento di ingengeria meccanica ed aerospaziale ne l CFD-LAB. L'argomento alla base dell'intership e quindi della presente tesi e' il rilevamento sia per via sperimentale del consumo energetico del sistema CFJ. Il lavoro alla base dell'intership e' stato svolto per conto del Dr.Gecheng Zha che mi ha dato la possibilita' di lavorare con il suo team di Ph.D. e di sfruttare le risorse a loro disposizione in particolare i computer ed i supercomputer ed il codice FASIP per quanto riguarda la parte computazionale ed il laboratorio del Wind-Tunnel (con annesse attrezzature laser per la P.I.V.)per quanto riguarda la parte sperimentale. Il codice FASIP e' un codice $Fortran^{TM}$ interamente sviluppato presso il CFD-LAB della Univ. of Miami sotto la supervisione del Dr.Gecheng Zha. L'acronimo CFJ sta per *tecnica di controllo del flusso attorno al profilo alare mediante flusso a getto*. Tale tecnica consente di migliorare le prestazioni di un dato profilo alare di base in termini di incremente di AoA e C_L e riduzione del C_D. La tecnica CFJ e' stata completamente sviluppata nel CFD-lab dell'Univerista' di Miami sotto la supervisione delDr.Zha. Il profilo alare usato per realizzare la tecnica CFJ e' un NACA6415 dal quale asportando un certo spessore della superficie superiore e creando opportune bocche di aspirazione e iniezione di aria si ottiene il profilo CFJ. All'interno del profilo alare vengono poi realizzate 2 cavita' una di iniezione e l'atra di risucchio entrambe collegate alla sezione di iniezione e risucchio di una pompa collocata nella parte centrale dell'ala. L'obiettivo ultimo e' creare un flusso sulla superficie superiore del profilo alare che tenga il piu' possibile attaccate alla superificie alare le linee di flusso che scorrono attorno all'ala stessa. In questa maniera, precedenti studi hanno dimostrato che le prestazioni del profilo alare, a parita' di numero di Mach e di condizioni atmosferiche si incrementano notevolmente. Tali prestazioni sono rappresentate principalmente dal coefficiente di portanza C_L, da quello di resistenza C_D e dall'angolo di Stallo AoAs. C_L e AoAs subiscono un notevole incremento invece C_D dimunuisce e per particolari angoli d'attacco diventa negativo. Un tipico aereo commerciale con catteristiche medie potrebbe arrivare a risparmiare fino al 10% di combustibile grazie alla tecnica del CFJ. La tecnica CFJ per essere attuata richiede una certa spesa di energia per attivare la pompa nell'ala, in particolare tale energia e' quantificata in termini di potenza assorbita che nel caso della pompa e' proporzionale alla portata

mandata ed alle pressioni nelle cavita' di iniezione ed aspirazione presenti nell'ala. Al fine di generalizzare i risultati della ricerca e di renderli indipendenti dalle grandezze tipiche del flusso libero che investe l'ala e cioe' la densita', la velocita' del flusso e dalle diemsnsioni dell'ala si e' scelto di calcolare il cosiddetto coefficiente di potenza P_c, un parametro adimensionale nella cui formula rientrano tutti i parametri della pompa,del flusso libero e la dimensione caratteristica dell'ala . Per il calcolo di tale coefficiente si sono prima di tutto effettuati rilevamenti sperimentali che sono serviti a validare simulazioni di al computer di alcune condizioni di funzionamento del CFJ. In particolare si sono scelti tre numeri di Mach 0.04, 0.07 e 0.01 , 3 AoA: 0^{circ}, 10^{circ}e 20^{circ} e si e' fissata la forza del getto iniettato sull'ala stabilendo un certo valore del parametro Cmu. Il Cmu e' proporzionale alla portata massica ed alla velocita' del getto iniettato sul profilo alare. Esso e' un parametro adimensionale visto che sia il numeratore che il denominatore hanno le dimensioni di una forza. Il lavoro di ricerca ha coperto un arco temporale di 7 mesi e mezzo durante il quale sono stati condotti lavori preliminari sia dal punto di vista sperimentale che computazionale. Innaznzitutto si e' condotto uno studio analitico e terorico del CFJ per capire quali grandezze dovessero essere prese in considerazione durante il successivo lavoro di ricerca. Questo studio si e' basato sulla dimostrazione delle formule del P_c e C_μ, sull'applicazione dell'equazione della quantita' di moto al profilo alare per calcolare le forze di reazione prodotte dalle aperture di aspirazione e risucchio dato che tali forze vanno a modificare formalmente le definizioni di C_L e C_D normalmente usate per un profilo alare base privo di CFJ. La presenza di tali forze di reazione spiega il funzionamento del CFJ. Un ultimo aspetto dello studio analitica e' stata la adimenzionalizzazione di tutte le grandezze temodinamiche perche' il codice FASIP lavora solo su tale tipo di grandezze. In questa maniera e' possibile infatti incrementare la precisione dei calcoli riducendo l'errore di round-off ed ottenere soluzioni simili. La spiegazione di questi concetti non immediata. Di consegueza anche le equazioni di Navier-Stokes, C_μ e P_c sono state riformulati in funzione dei parametri non dimensionali. Dal punto di vista sperimentale sono state eseguite delle rilevazioni mediante P.I.V. e sono state eseguiti vari test per capire dove e come collocare i tubi di Pitot all'interno del profilo alare CFJ visto che le cavita' di aspirazione e risucchio all'interno dell'ala non consentono un facile assemblaggio dei sensori. Tali sensori sono seriviti per misurare le pressioni totali nelle cavita' nonche' la temperatura totale del flusso indisturbato all'interno del Wind-Tunnel. Per quanto riguarda la fluidodinamica numerica sono state eseguite alcune simulazioni su dei semplici casi-benchmark come la lastra piana investita da flusso supersonico e subsonico, il profilo RAE2822 ed il profilo M6. I risultati di tali simulazioni sono stati confrontati con i corrispondenti risultati numerici per testare l'accuratezza del codice. Tali risultati riguardano i profili di velocita' e temperatura in prossimita' della superficie del corpo investito da un flusso d'aria turbolento e l'andamento del coefficiente di pressione lungo la superficie del corpo. Inoltre sono state riprodotte sia in via sperimentale che numerica anche le curve del C_L e C_D del profilo base NACA6415 come utile confronto rispetto alle stesse ottenute per il CFJ ed inoltre si e' dovuto sviluppare un codice fortran per eseguirir il postprocessing dei dati al fine del calcolo di C_L, C_D e P_c. Il profilo CFJ oggetto della ricerca e' un caso particolare denominato CFJ-open slot in quanto l'apertura

dalla quale e' iniettato il getto non e' frazionata mediante i tacche metalliche. In totale sono stati considerati 9 casi di studio, come gia' detto prima, cioe' per un dato AoA si sono considerati tre differenti numeri di Mach del flusso libero. Per un dato caso di studio sono state rilevate le curve del C_L, del C_D e sono state rilevate tutte le grandezze necessarie a calcolare il P_c la cui formula e' stata ottenuta mediante il precedente studio analitico sfruttando il primo principio della termodinamica. Per quanto riguarda il lavoro computazionale, sono stati creati 2 modelli bidimensionali, uno per il profilo base NACA6415 ed uno per il profilo CFJ. Le due geomentrie sono state create usando un software cad, dopodiche' sono state importate nel software Gridgen V15 dove e' stat generata la mesh, in particolare il tipo di mesh usato e' una o-mesh con quadrilateri. Il profilo base NACA6415 ha una mesh composta di 15 superfici in totale mentre il profilo CFJ si compone di 19 superfici. Per ciascun AoA la mesh e' stata opportunamente ruotata in Gridgen prima di esere fornita in input al codice. Per realizzare quest'ultimo obiettivo e' stato necessario utilizzare una applicazione, il plot3d2ransche converte la mesh in file binari. Dopodiche', per ciascun caso di studi sono stati forniti in input il file datain contenente le condizioni al contorno ed i valori delle grandezze fluido e termodinamiche utili. La procedura di calcolo prevede di inserire in un file chiamato init.input i valori della temperatura e pressione totale della cavita' di iniezione ed il valore della pressione statica nella cavita' di risucchio. Dopodiche" viene lanciata la simulazione sfruttando il codice FASIP e quindi i risultati vengono rielaborati mediante un codice di post-processing. A questo se le portate massiche di aspirazione e risucchio sono circa uguali entro un range del 2% e se il valore del C_μ attuale e' abbastanza vicino a quello ideale pari a 0.042 il calcolo puo' considerarsi terminato. Altrimenti si rende necessario modificare i valori inseriti in init.input. I risultati ottenuti dal codice di post-processing sono stati inseriti nel software TECPLOT mediante il quale e' stato possibile ottenere i grafici e i contour del profilo alare. I contour sono stai utili per verificare la fisica del flusso attorno al profilo alare e per rilevare eventuali zone di ricircolo. In questo modo e' stato possibile verificare la plausibilita' fisica dei risultati numerici. Per ogni simulazione e' stato raprresentata la storia di convergenza. Ciascun calcolo e' stato considerato valido se ha subito una caduta dell'ordine di grandezza del residuo pari a circa 5 punti. Complessivamente, i risultati della ricerca sperimentale mostrano che il CFJ apporta un migliormanento del C_L di circa il 13% a 0°, 19% a 10° and 18% a 20°. Dal punto di vista computazionale l'aumento medio del C_L e' di circa il 22% at 0°, 21% a 10° ma non ci sono miglioramenti a AoA 20° a causa dello stallo. Confrontando i risultati sperimentali con quelli computazionali si osserva che in questi ultimi lo stallo interviene prima perche' i modelli numerico-matematici usati dal codice non sono in grado di catturare a pieno la natura statistica della turbolenza. Per piccoli valori dell'AoA la portanza viene sopravalutata di circa il 15% nel caso CFJ. Risultati simili sono stati osservati nel caso del profilo base. I dati sperimentali mostrano una riduzione della D fino al 45% per mach M1 cosa che non si e' osservata per M2 ed M3. I risultati computazionali mostrano che per alti M, la D si riduce ed addirittura tende ad annullarsi per AoA 0°. Paragonando i risultati CFD ed sperimentali si osserva che specie per M2 ed M3 , la D del caso CFJ risulta molto vicina a quella del profilo base. La sostanziale differenza tra i risultati CFD e quelli sperimentali si

suppone sia causata dalle imperfezioni superficiali del profilo alare usato nel Wind Tunnel. Come visto nell' Eq.4.21 la potenza richiesta e' funzione di $\dot{m}_j$, V_j e Γ. I valori computazionali di $\dot{m}_j$ e V_j sono molto simili a quelli si Fig. 6.21 e Fig. 6.24. Come ci si aspettava, $\dot{m}_j$ e V_j aumentano con la velocita' del flusso libero in modo che C_μ resti costante. Se la forza del getto aumenta $\dot{m}_j x V_j$, Γ aumenta come mostrato in Fig **??**. Computazionalmente possiamo osservare che Γ e' basso per AoA 0° e 10° ed aumenta per AoA 20°. Per piccoli AoA parte dell'energia del getto raggiunge la coda dell'ala facilitando l'aspirazione; questo risulta piu' difficile er alti AoA. Infatti e' stato mostrato in Fig. 6.28 che l'energia del getto e' dissipata a causa della turbolenza nella coda del profilo alare. I risultati computazionali sottovalutano lievemente il Γ e si scostano di circa il 4% rispetto ai risultati sperimentatali. Essensoil Γ piccolo, anche il P_c risulta piccolo, come mostrato in Fig.6.23. Il P_c per un prefissato C_μ varia di poco sia col M che con AoA. Questo evidenzia la bonta' di C_μ eP_c nel rappresentare una prefissata condizione di funzionamento del sistema CFJ.

Chapter 2

Introduction

2.1 Introduction

An active flow control(FC) method is to enhance airfoil performance by energizing the flow with minimal or no structural moving parts. When a high lift airfoil flow control technique is developed, three primary issues need to be considered: 1) effectiveness, 2) energy efficiency, and 3) ease of implementation. First, the FC method should provide a substantial improvement in aerodynamic performance, which may include lift enhancement, drag reduction, and stall margin increase. Second, the FC method should not require significant energy expenditure. Otherwise, the penalty may outweigh the benefit for the whole aircraft system. Third, the FC technique should not be too difficult to implement. Various FC approaches are briefly summarized below.

The rotating cylinder method [10, 11] is generally most effective when the leading edge (LE) or trailing edge (TE) are thick and, hence, may be more applicable to low-speed airfoils. This approach requires a rotating drive system, which increases aircraft weight and potentially reduces the net efficiency of the approach. An improved approach is the circulation control (CC) airfoil, which was originally developed for helicopter airfoil lift enhancement [12].

The circulation control airfoil [12–14] relies on the Coanda effect, which creates a locally favorable pressure gradient on a curved surface to attach the flow. Such a favorable pressure gradient exists at the airfoil LE due to suction and in the vicinity of a blunt TE due to the low base pressure. Hence, a blunt TE is usually required to render CC effective. However, this will create large drag at cruise conditions. To overcome the dependence on a blunt TE for circulation control airfoil, a movable flap at the airfoil TE has been suggested by Englar [15]. Unfortunately, such moving parts impose a weight penalty. At large angles of attack (AoA), the flow cannot overcome the large adverse pressure gradient. As a result, a favorable pressure gradient near the TE cannot be achieved and, hence, the Coanda effect is difficult to realize. If only TE blowing is used, a circulation-controlled airfoil will stall at a smaller AoA than a non-controlled airfoil [16]. To maintain sufficient stall margin, LE blowing also needs to be added [16].

A considerable penalty of CC is the dumped blowing jet mass flow, which is

imposed on the propulsion system. This is because the supply air for control is usually obtained from the engine compressor bleed. The resultant decrease in thrust is directly proportional to the mass flow rate of the engine bleed; i.e., an engine will incur a 1% thrust decrease for a 1% bleed flow and will result in a 1-3% fuel consumption increase depending on whether the bleed is from the compressor front or back stage. Furthermore, for a CC airfoil, the drag measured in the wind tunnel is not the actual drag that will occur on the aircraft. This is because, in the wind tunnel, the penalty to draw the mass flow from the freestream as the supply for the jet injection is not included in the drag measurement. The actual drag, also called the "equivalent" drag, needs to include this penalty [17, 18]. The penalty to draw mass flow from the freestream includes ram drag and captured area drag. The equivalent drag of a CC airfoil is thus significantly larger than the drag measured in the wind tunnel [17].

To reduce the penalty associated with CC due to the dumped jet mass flow and the equivalent drag, a pulsed jet can be used [18] and is able to significantly reduce the jet mass flow rate. Recently, other promising methods using zero-net mass flux (ZNMF) synthetic jets [19, 20] and dielectric-barrier discharge plasma actuators [21, 22] are being developed. These approaches avoid dumping the jet mass flow. However, at present, both ZNMF and plasma actuators are generally lacking in terms of sufficient actuator authority for high speed flows.

Recently, a promising ZNMF co-flow jet flow control airfoil based on fluidic actuators (hereafter co-flow jet airfoil or CFJ airfoil) has been developed by Zha et al. [17,23–28]. The CFJ airfoil achieves three effects simultaneously in a radical manner: lift augmentation, stall margin increase, and drag reduction. The CFJ airfoil performance enhancement is much more significant than all of the other aforementioned flow control methods. The energy expenditure of the CFJ airfoil is low [17,28], and the CFJ airfoil concept is straightforward to implement.

2.2   The ZNMF CFJ Airfoil

In the CFJ airfoil concept [17,23–28], an injection slot near leading edge and a suction slot near trailing edge on the airfoil suction surface are created as sketched in Fig. 2.1. A small amount of mass flow is withdrawn into the airfoil near the trailing edge(TE), pressurized and energized by a pumping system inside the airfoil, and then injected near the leading edge(LE) in the direction tangent to the main flow. The whole process does not add any mass flow to the system and hence is a ZNMF flow control.

The CFJ airfoil flow process provides a unique low energy expenditure ZNMF flow control, which has the injection near the suction peak of the airfoil where the lowest main flow pressure is located, and jet suction at the near trailing edge where the highest main flow pressure is located. In other words, the required pumping work of CFJ airfoil would be lower than those of the flow control methods injecting near trailing edge such as a CC airfoil. Furthermore, a flow control method using injection only will have to do more work to overcome the ram and captured area drag, which do
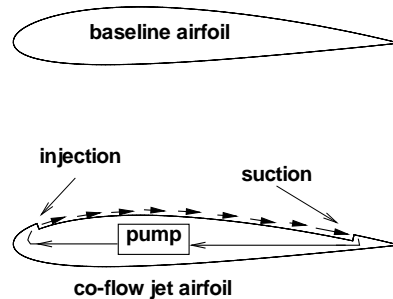
Figure 2.1: Baseline airfoil and CFJ Airfoil.

Figure 2.2: Massive flow separation of baseline NACA 6415 airfoil at AoA=25°.
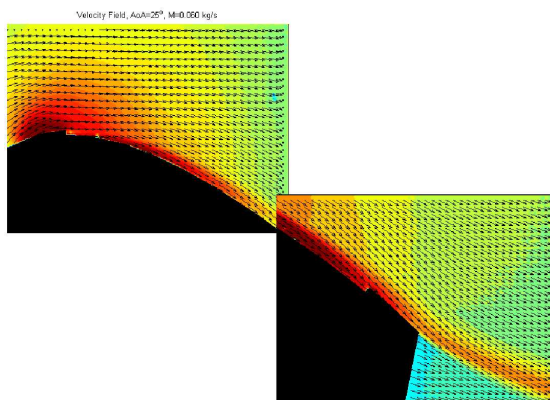
Figure 2.3: Attached flow of CFJ NACA 6415 airfoil at AoA=25° measured by PIV in experiment.
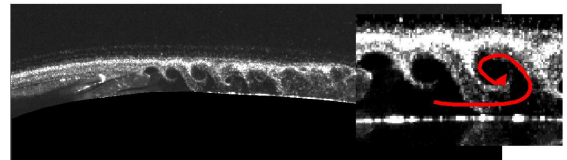
Figure 2.4: Coherent vortex structures in the region of CFJ airfoil injection, AoA=5°, $C_\mu = 0.02$.

not exist for CFJ airfoil due to the ZNMF [17]. As pointed out in [17], the injection and suction of CFJ airfoil are efficiently integrated and they both enhance boundary layer momentum and airfoil circulation. Most of other flow control methods will suffer greater penalties at suction process either due to ram drag, captured area drag or larger flow ducting loss.

The fundamental mechanism of CFJ airfoil is that the turbulent mixing between the jet and main flow makes a lateral transport of energy between the jet, boundary layer, and main flow to energize the wall boundary layer. The large vortex structures and adverse pressure gradient are all beneficial to enhance mixing. The mixing allows the flow to overcome a large adverse pressure gradient and remain attached at a very high angle of attack. Hence, the stall margin is significantly increased. At the same time, the energized boundary layer drastically increases the circulation, augments lift, and reduces the total drag or generates thrust (net negative drag). The portion of

CFJ energy used to overcome the increased local drag due to higher jet speed is small since the mixing occurs immediately when the jet penetrates into the boundary layer under an adverse pressure gradient. Unlike a jet in cross flow (JICF) which enhances mixing between the jet and main flow but retards the main flow due to the cross flow blockage created by the jet, the co-flow jet mixing only enhances the stream-wise flow momentum since the jet is tangential to the main flow. The momentum retardation due to JICF will result in a significant entropy and drag increase.

The thrust generation or drag reduction by a CFJ airfoil can be explained by two mechanisms [17, 23–25]: First, due to the very high circulation, the LE suction is so strong that the low pressure at the LE results in a thrust when the AoA is below a certain value. The slightly increased local surface friction due to higher jet velocity is offset by this LE super-suction, or pressure drag reduction, which is the same mechanism that bird wings generate thrust at down stroke flapping at high AoA. Second, the energized main flow fills the wake and reduce velocity deficit. From control volume analysis, it is known that a shallower wake velocity deficit means a smaller drag. When the wake velocity deficit is reversed, the airfoil will generate a thrust, which occurs for CFJ airfoil as demonstrated in both experiments and numerical simulation [17, 23–28]. CFJ airfoil appears to be the only flow control method that generate both significant lift and thrust at the same time. It is because a CFJ airfoil is benefited greatly from the tangential jet injection momentum even though the jet suction will offset the benefit. Fig. 2.2 shows a massive flow separation of baseline NACA 6415 airfoil at AoA of 25° in our wind tunnel testing [27]. Fig. 2.3 is the PIV measured velocity field with CFJ at the same AoA, which demonstrates that the flow is attached with a higher speed within the wake than in the free-stream, a reversed wake deficit or jet. In this case, a thrust is generated. The flow is attached at a momentum coefficient C_μ of 0.06 for this case.

Fig. 2.5 compares the lift coefficient of CFJ airfoils with baseline airfoil at the momentum coefficient $C_\mu = 0.08$. The CFJ airfoils have different slot blockages to generate discrete holes and hence different jet velocity while keeping the same mass flow rate. For example, the open slot (black solid circles) has zero blockage. The symbol OF stands for the obstruction factor (blockage), which is the percentage of the slot area blocked. OF of 3/4 means that 75% of the injection slot area is blocked and it results in many small discrete holes for the CFJ injection. Fig. 2.5 shows that the open slot CFJ airfoil increases the maximum lift coefficient by about 50%, whereas the discrete CFJ airfoil with OF of 2/3 increases the lift by about 100%. When the momentume coefficient is increased, the maximum lift coefficient is further augmented.

A unique feature of CFJ airfoil is it generates a large thrust while increasing the lift due to efficient energizing stream-wise momentum of the flow. Fig. 2.6 shows all the airfoils generate thrust (negative drag) with the maximum amount produced by a CFJ airfoil using discrete jets with obstruction factor of 3/4. The minimum drag is reduced by 4000% to a enormous thrust coefficient of about 0.8. By comparing with the open slot CFJ airfoil, the discrete CFJ (DCFJ) airfoil needs half of the mass flow rate to achieve the same lift augment and drag reduction [28]. However, the power consumed by the DCFJ is significantly higher than the open slot CFJ airfoil since the

smaller holes create more blockage loss for the jets. Nonetheless, the extraordinary high lift and high thrust generated by the DCFJ deserve the extra energy cost [28]. In nature, the only system that generates both lift and thrust at the same time is bird flapping wings. In the man made world, no other airfoil or flow control methods other than CFJ airfoil can generate both significant lift and thrust at the same time.
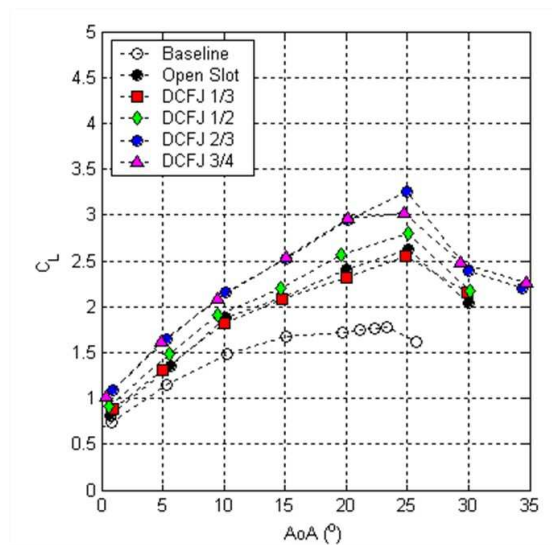
Figure 2.5: Comparison of lift coefficient of CFJ airfoils with different obstruction factors, $C_\mu^* = 0.08$.
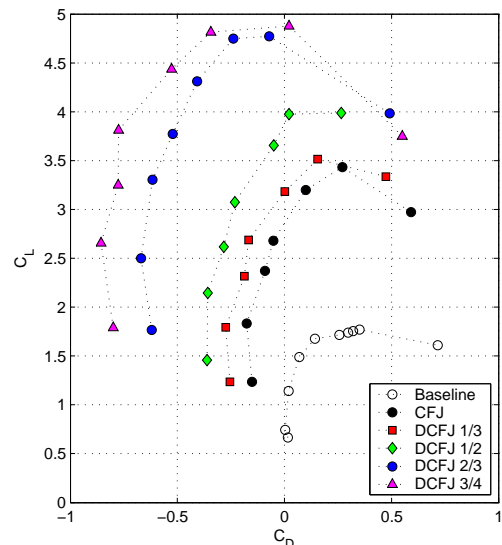
Figure 2.6: Comparison of the drag polars of discrete CFJ airfoils with different obstruction factors, $C_\mu^* = 0.25$.

Even though CFJ airfoil shows great potential to enhance the airfoil performance, it is important to study the energy expenditure of the airfoil due to the flow control. Dano et al [28] investigate the expenditure of the CFJ airfoil at Mach number of 0.03, which indicates that the CFJ airfoil gain tremendous performance enhancement at high angle of attack at low energy expenditure.

2.3   Purposes if the research

The purpose of this thesis is to study the CFJ airfoil energy expenditure with the variation of Mach number for M equal to 0.04, 0.07 and 0.1, for different AoA, in particular 0°, 10∘ and 20° and keeping constant $C_\mu = 0.042$. It is important to understand this performance so that the CFJ airfoil can be applied to higher Mach number such as for helicopter blades. The finding of the research is that the power coefficient of the CFJ airfoil does not vary much with Mach number, which is desirable.

$$C_\mu = \frac{\dot{m} V_{jet}}{\frac{1}{2}\rho_\infty V_\infty{}^2 S} \tag{2.1}$$

where $\dot{m}$ is mass flow rate, V_{jet} is jet velocity, ρ_∞ and V_∞ are free stream density and velocity respectively, and S is the span area of the airfoil. A Co-Flow Jet Wind Tunnel Laboratory was designed and constructed at the University of Miami to obtain experimental CFJ data. The results of the CFD analysis and experimental data are compared to demonstrate the CFJ airfoil performance enhancements. The FASIP (Fluid-Acoustic-Structure Interaction Package) CFD code, developed at the University of Miami CFD Laboratory, was used to obtain numerical results [29–41].

Chapter 3

Baseline and Co-Flow Jet Airfoils description

3.1 Introduction

Some geometrical modifications are needed on the baseline airfoil profile in order to obtain on the wing all the features necessary to make the CFJ system working. This chapter contains some basic information about the baseline and the CFJ airfoil.

3.2 The base-line airfoil profile NACA6415

The starting point of the research is the baseline profile, the NACA6415, this is a thin cambered airfoil and it was chosen for this research to demonstrate that co-flow jet implementation is possible for any airfoil thickness. Previous studies of wind tunnel experiments and CFD analysis have been done using a NACA 0025 airfoil, which is thicker and symmetric [3, 5, 6, 8, 9, 42, 43]. The NACA 6415 airfoil was used for the baseline shape and as a guide for the translation of the suction surface to become a CFJ airfoil. The acronym NACA6415 stands for:

- 6: maximum ordinate of the mean line;

- 4: position of the maximum chamber;

- $15 = t_{max}/c$

- c=12in (chord)

- s=24inc (span)

It is possible to see in the figure above that the chord $c = 1$, this is a reference value used into the meshed model of the wing used during the numerical calculations. Coordinate data was used from a NACA 6415 airfoil as the baseline shape of the CFJ airfoil. The following equations are used to obtain the coordinates of an airfoil and are given by Abbott and Von Doenhoff [44]. The mean line is found using two

7
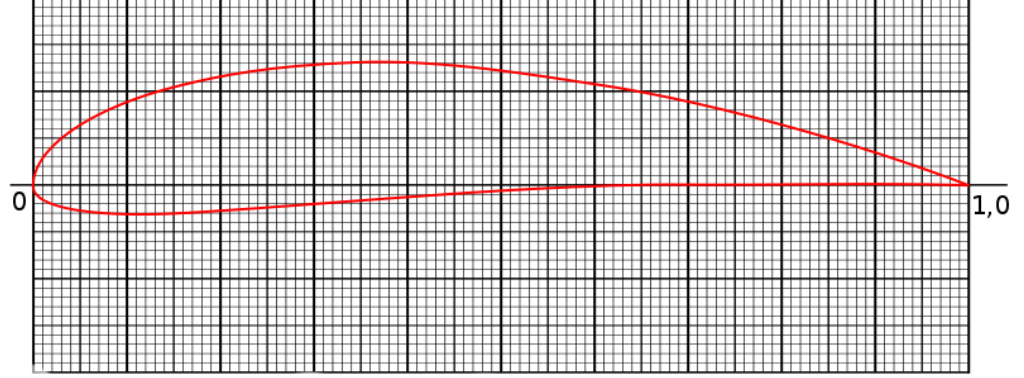
NACA 6415

Figure 3.1: NACA6415 AIRFOIL PROFILE

functions, one for values forward of the max ordinate and one for values aft. These are shown in Eq. (3.1) and Eq. (3.2) respectively,

$$y_c = \frac{m}{p^2}\left(2px - x^2\right) \quad \text{forward of max ordinate} \tag{3.1}$$

$$y_c = \frac{m}{(1-p)^2}\left[(1-2p) + 2px - x^2\right] \quad \text{aft of max ordinate} \tag{3.2}$$

where m is the maximum ordinate of the mean line and p is the chord-wise position of the maximum ordinate. the non-dimensional chord-wise dimension, x varies from 0 to 1 and for the NACA 6415, $m = 6$ and $p = 4$. Next, the thickness distribution is given by Eq. (3.3), where t is the maximum thickness of the airfoil as a percent of the chord length ($t = 15$ for NACA 6415).

$$y_t = \frac{t}{0.20}\left(0.2969\sqrt{x} - 0.1260x - 0.3516x^2 + 0.2843x^3 - 0.1015x^4\right) \tag{3.3}$$

Finally, the coordinates of the upper and lower surface of the airfoil can be found using Eq. (3.4) and (3.5) for the upper surface and Eq. (3.6) and (3.7) for the lower surface. Eq. (3.8) shows the value for θ in these equations as the angle slope of the mean line. [43]

$$x_U = x - y_t sin\theta \tag{3.4}$$

$$y_U = y_c + y_t cos\theta \tag{3.5}$$
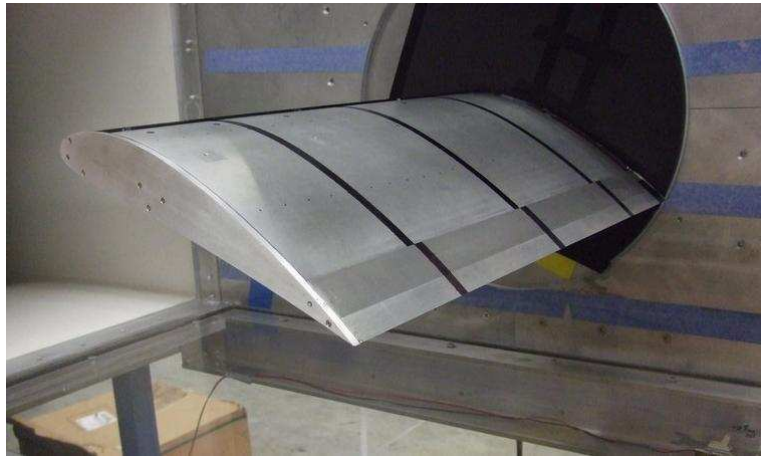
Figure 3.2: NACA6415 AIRFOIL PROFILE

$$x_L = x + y_t sin\theta \tag{3.6}$$

$$y_L = y_c - y_t cos\theta \tag{3.7}$$

$$\theta = tan^{-1}\left(\frac{dy_c}{dx}\right) \tag{3.8}$$

These equations give coordinates for the baseline shape of a NACA 6415 airfoil. Here below there is a photo of the true wing that we used on the CFD lab, into the Wind tunnel.

3.3 CFJ-6415 geometry and technical data

As we said before, the CFJ6415 is a modification of the original baseline profile. Also in the case of the CFJ profile there is a convention that is based on the one of the baseline profile. The acronym in this case will be structured as $CFJ6415 - h_{inj} - h_{suc}$. There are some important features that must specified, keeping in mind that the span s, the c and also the *4-digit convention 6415* are the same of the baseline profile:

- 6:maximum ordinate of the mean line;

- 4;position of the maximum chamber;

- $15 = t_{max}/c$;

- $c = 12in$ (chord);

- $s = 24inc$ (span);

- θ_1=26.67°(injection slot jet angle);
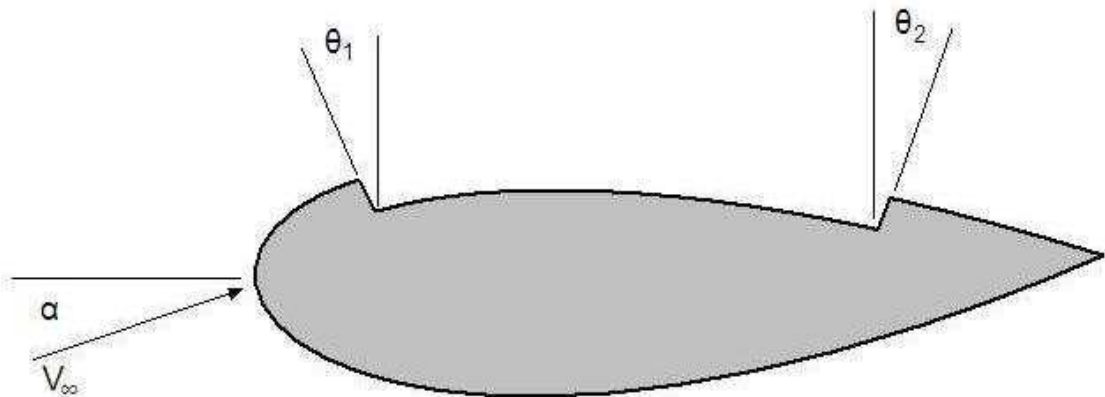
Figure 3.3: Jet angles

- θ_2=40.60°(suction slot jet angle);

- h_inj=65 (injection slot height as a percentage of the chord);

- h_suc=142.(suction slot height as a percentage of the chord)

The figure below give a clear explanation of the meanings of all these features.

The wing's material is machined aluminum. The h_inj and h_suc are measured as the distance of the openings normal to the upper curved surface of the baseline airfoil. The injection and suction slot heights are 0.65% and 1.42% of the chord, respectively. Previous studies show that an injection slot height of this size provides better performance results than a thicker injection slot [3, 8]. The thinner injection slot has a lower mass flow rate and requires less power from the compressor bleed. The suction slot is larger so that the same mass flow expended by the injection slot can be removed by the suction slot without choking, due to the lower static pressure achieved by the vacuum. The location of the injection and suction slots were also determined from previous works. The injection slot should be located as close to the leading edge as possible but still downstream of the suction peak on the airfoil [6]. This positioning takes advantage of the severe adverse pressure gradient and uses it to promote mixing between the jet at the wall and the main stream flow. The injection and suction slots are located at 7.5% and 88.5% of the chord, respectively. Description of the airfoil design includes exterior coordinate generation for baseline and CFJ airfoils, development of interior cavities required for the CFJ airfoil, and CAD modeling to create an adjustable slot size wind tunnel model with connection to a side mounted force balance. The co-flow jet slots were generated from the baseline coordinates. The upper surface was translated downward to create the CFJ geometry. Since the injection and suction slot have different thicknesses, two translations were made and a resulting surface was created by blending the two together. Each y-coordinate was generated by introducing a rotation angle between each point. The

resulting blended surface became the suction surface of the CFJ airfoil. The original translated surfaces were simply shifted vertically downward by the thickness of the injection and suction slot. The coordinates for the baseline NACA 6415 and the CFJ 6415-065-142 airfoil are given in Appendix A. Plots of the baseline NACA 6415, the two translated surfaces for the injection and suction slots, and the final CFJ airfoil cross section are also included. Some design parameter both for the Wind-tunnel facility and for the wing are given here:

- maximum Mach number for the wind tunnel free stream M=0.1;

- max injection jet force is given by $C_\mu = 0.4$;

- $V_{jet} = 3 \cdot V_\infty$ (V_∞=free stream velocity, V_{jet}=jet velocity);

All the values of the free stream are referred to standard conditions:

- $\rho_\infty = 1.23\,\mathrm{kg/s}$;

- $V_\infty = 34.55\,\mathrm{m/s}$;

- $T = 297.04\,K$

- $R = 287.06\,J/(kg \cdot K)$

Some useful relation for the design of the CFJ profile internal ducting are given here below, keeping in mind that the guideline is to avoid that the flow in all the cavities get chocked:

$$\dot{m} = \frac{C_\mu \frac{1}{2}\rho_\infty V_\infty^2 S}{V_{jet}} \tag{3.9}$$

$$V_\infty = M \cdot a \tag{3.10}$$

$$a = \sqrt{\gamma\,R\,T} \tag{3.11}$$

The solid section in the center of the airfoil connecting the injection and suction cavities was made thinner to reduce material and the model's weight. The larger area in the injection cavity was used for the air delivery apparatus and the force balance mounting. These features and others are discussed further in the next section. The upper section of the injection cavity was also made thinner for the same reasons. In addition, the converging area leading to the jet was made with a lower slope and the curving walls that turn the flow were made with a larger radius so that all streamlines could easily exit the jet without forming internal stagnation points. The cut-outs in the injection cavity are for the placement of Duocel® aluminum foam. Since the air enters the CFJ airfoil from the side, the foam is essential to make the flow uniform as it exits the jet. Density comes from a maximum cavity total pressure of 80 psi (551.6 kPa) and ambient temperature of 75°F (23.9°C) In the injection cavity, the pressure will increase as C_μ increases. Also, the increased $\dot{m}$ will require higher pressure. The pressure can be regulated by controlling the amount of flow entering the cavity from
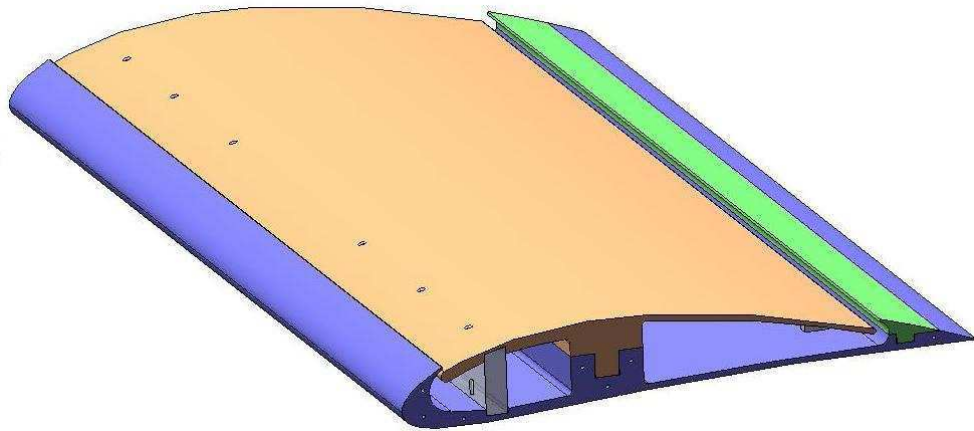
Figure 3.4: The CFJ airfoil profile

the air delivery system. The minimum 2-D area for the injection cavity is therefore not as critical as the minimum area for the suction cavity, because the pressure will increase as mass flow increases on the injection side. As air flows out of the holding tank at high mass flow rates, the decrease in temperature will not be of concern because the high pressure will mediate the density and maintain the minimum area required. A worst case scenario combination of pressure and temperature was chosen to find density and ultimately find the minimum injection area. Eq. (3.13) is the state equation for an ideal gas as it is solved for density. The minimum area was found to be $0.3843\,in^2$ ($2.479 \times 10^{-4}\,m^2$) for the injection cavity. [43]

$$\dot{m} = \rho\,V A \tag{3.12}$$

$$\rho = \frac{p}{R\,T} \tag{3.13}$$

Chapter 4

Analytical study of CFJ

4.1   Introduction

The first step of this research was to study the forces acting on the CFJ wing during a flight because this kind of analysis permit to understand what are the improvements that the CFJ method brings. In a normal baseline profile during a flight at a fixed altitude and traveling at constant velocity V_∞ the pressure distribution all around the wing produce as resultants a Lift and a Drag forces as explained in Fig. 4.1

Into the local frame of the wing, the wing itself is immobile and it is immersed in a flow that at very long distance is not influenced by the wing and so it is called *free-stream*. Into the CFJ wing the presence of the injection and suction jets introduce some reaction forces that modify the magnitude both of the Lift and the Drag.

4.2   Jet effects on CFJ performances

A control volume analysis was performed to study the effects of the CFJ. A rectangular control volume all around the wing was chosen like the one shown in Fig. 4.2 .

The control volume is individuated by the points **abcdefghia**. In the picture the one on the left is the free stream flow that comes into the control volume from the inlet and exits from the control volume at the outlet on the right side. This flow is perpendicular both to the inlet and the outlet boundaries and it is parallel to the upper and lower boundaries. The pressure distribution all around the control volume, along the boundaries **abhi**, is uniform and equal to the one of the free stream. Also the outline of the wing represents a boundary for the control volume and in particular we have to consider that a jet is injected from slot 1 into the control volume and the same amount of mass flow is sucked into the airfoil at the slot2. The Momentum equation was applied to the control volume, its general form is

$$\sum F = \iint_S \rho \mathbf{V} \cdot \mathbf{dS} \cdot \mathbf{V} \tag{4.1}$$

The left hand side of the last equations is the resultant of the forces applied on
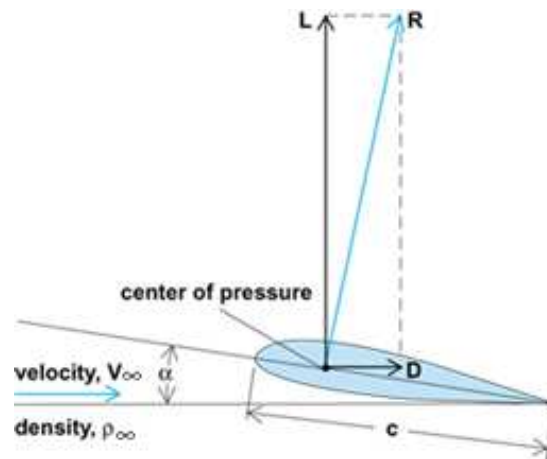
Figure 4.1: Forces acting on a common baseline airfoil profile
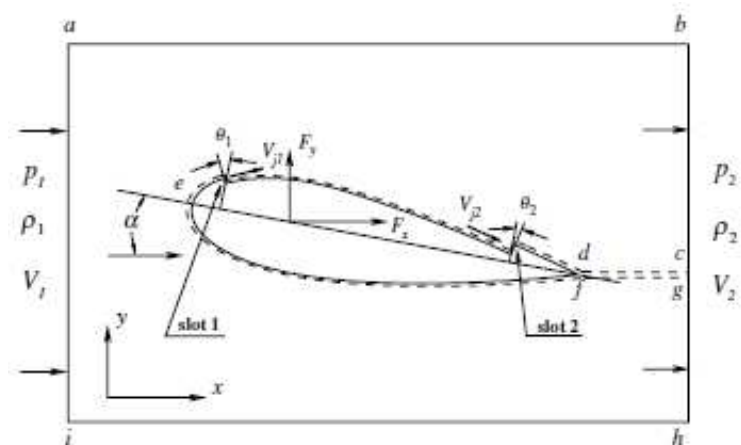
Figure 4.2: Control volume for a CFJ airfoil

the control volume while the right hand side of this equation represents the variation of momentum across the boundaries of the control volume.

$$-p_e + p_\infty A_\infty + (p_{inj} A_{inj})_x - (p_{suc} A_s uc)_x + R_x = \int_h^b \rho V_e dy V_e - \int_i^a \rho V_\infty - \dot{m}_{inj} u_{inj} + \dot{m}_{suc} u_{suc}$$
(4.2)

Because $p_e = p_\infty$ and $A_e = A_\infty$ the first two terms in the above equations, on the left hand side, are canceled. The jets reactionary forces can be obtained by choosing a convenient control volume between the injection and suction slot. The component of the resultant reactionary force along x-ax is:

$$F_x = (\dot{m}_j V_{inj} + p_{inj} A_{inj}) * cos(\theta_1 - \alpha) - \gamma(\dot{m}_{suc} V_{suc} + p_{suc} A_{suc}) * cos(\theta_2 + \alpha) \quad (4.3)$$

$$F_y = (\dot{m}_j V_{inj} + p_{inj} A_{inj}) * sin(\theta_1 - \alpha) - \gamma(\dot{m}_j V_{suc} + p_{suc} A_{suc}) * sin(\theta_2 + \alpha) \quad (4.4)$$

In the specific case of the CFJ6415-065-142, the angles values are $\theta_1 = 26°$ and $\theta_2 = 40°$. To develop the momentum equation on the control volume it is necessary to individuate on the injection surface a unity vector with magnitude equal to 1 that goes out of the control volume and that is normal to the slot section, than starting from the vectorial form of the momentum equation it is possible to develop each integral term using the dot product and keeping in mind that the **dS** that appears into the integrals is the unity vector. The Drag is due to two contributes:

- $R'_x = -R_x$:airfoil surface drag;

- $-F_{xcfj}$:reactionary force in drag direction (x) due to injection and suction slots.

so the total drag will be:
$$D = R'_x - F_{xcfj} \quad (4.5)$$

Now by substituting the F_{xcfj} expression in the last one it is possible to relate D to the velocities:
$$D = \int_i^a \rho V_\infty dy V_\infty - \int_h^b \rho V_e dy V_e. \quad (4.6)$$

The CFJ method works thanks to a pump that is a fluid machine that respects the conservation of the mass so:
$$\dot{m}_{inj} = \dot{m}_{suc} \quad (4.7)$$

and by using the definition of mass flow rate for developing the last relation as below:

$$\int_i^a \rho V_\infty dy = \int_h^b \rho V_e dy \quad (4.8)$$

then equation 4.6 becomes: $D = \int_h^b \rho V_e (V_\infty - V_e) dy$

From this last expression we can see that the Drag for a CFJ airfoil is calculated in the same way of a conventional airfoil without no CFJ; from the expression 4.3 we can see that the effect of the injection is to reduce the Drag because of the thrust induced by the jet while the effect of the suction is opposite.

The lift measured from the wind tunnel balance is

$$L = R'_y - F_{ycfj} \tag{4.9}$$

R'_y is the y-direction component of the surface pressure and shear stress integral induced by the circulation. F_{ycfj} is the suction slot reactionary forces. It is obtained in the same way of the F_{xcfj}.

$$F_{ycfj} = (\dot{m}_{inj}V_{inj} + p_{inj}A_{inj}) * sin(\theta_1 - \alpha) + \gamma(\dot{m}_j V_{suc} + p_{suc}A_{suc}) * sin(\theta_2 + \alpha) \tag{4.10}$$

from this last equation we can see that the suction almost always decreases the lift. The power required to to the pump to activate the CFJ is:

$$P_{cfj} = V_\infty F_{xcfj} = V_\infty[(\dot{m}_j V_{inj} + p_{inj}A_{inj}) * cos(\theta_1 - \alpha) - (\dot{m}_j V_{suc} + p_{suc}A_{suc}) * cos(\theta_2 + \alpha)] \tag{4.11}$$

From this last formula we can see that the power consumption is dependent from the free stream velocity , from the inclination of the slots (θ_1 and $theta_2$ and from the angle of attack of the wing αbut this is almost intuitive because as αincreases respect to the direction of the $_\infty$the frontal area of the wing increases and the Drag increases, this is due to the physics. In addiction the direction of the injection and suction jets ($\theta_1$and θ_2 determines also the direction of the reaction forces. [1]

4.3 The power calculation

The power requested to the CFJ pump is calculated by applying the 1stPT considering the thermodynamic variations between the inlet section (subscript 1) of the pump and the outlet section (subscript 2). to the control volume that is the whole mass of air that in a fixed time interval is into the pump. So the 1stPT equations will be:

- L_i is the work per unit mass that the air into the pump receives from the internal moving part;

- Q_e is the heat that the air into the pump exchange with the walls;

- $\Delta E_c = \frac{V_2^2}{2} - \frac{V_1^2}{2}$ is the air kinetic energy variation per unit mass;

- V_2 and V_1 are the air velocity at the outlet and inlet of the pump;

- ΔE_g is the air energy variation per unit mass due to the gravitational force;

- $\Delta E_c entrifugal$ is the air energy variation per unit mass due to the centrifugal forces;

- Δi is the variation of enthalpy per unit mass of air.

$$L_i + Q_e = \Delta i + \Delta E_c + \Delta E_g + \Delta E_{centrifugal} \qquad (4.12)$$

From the fluid dynamic theory about fluid machines it's possible to assume that $\Delta E_g = \Delta E_{centrifugal} = Q_e = 0$ and the Eq. 4.12 will become as below:

$$L_i = \Delta i + \Delta E_c \qquad (4.13)$$

where Air is treated like an ideal gas so under this hypothesis the enthalpy is proportional to the temperature of the gas. It is also possible to explicit the E_c as a function of the velocity so:

$$L_i = C_p(T_2 - T_1) + (\frac{V_2^2}{2} - \frac{V_1^2}{2}) \qquad (4.14)$$

by applying the definition of total enthalpy:

$$L_i = i_{02} - i_{01} \qquad (4.15)$$

and under the hypothesis of perfect gas:

$$L_i = C_p(T_{02} - T_{01}) \qquad (4.16)$$

and by factorizing the T_{01}:

$$L_i = C_p T_{01}(\frac{T_{02}}{T_{01}} - 1) \qquad (4.17)$$

It is possible to assume that the flow is is-entropic so under this hypothesis the relation between the termodynamics values betweenn the entering and the exit section of the pump, it is valid the relation below:

$$\frac{T_{02}}{T_{01}} = (\frac{P_{01}}{P_{02}})^{(\frac{\gamma-1}{\gamma})} \qquad (4.18)$$

where we use $\Gamma = \frac{P_{01}}{P_{02}}$ and the equation 4.17 becomes:

$$L_i = C_p T_{01}(\Gamma^{\frac{\gamma-1}{\gamma}} - 1) \qquad (4.19)$$

The power requested by the pump in ideal conditions (without losses into the machine) is the product between the work made by the pump on the unit of air mass that flow in the pump itself and the mass of air that flow across the pump in a unit of time so:

$$P_{id} = L_i \dot{m}_{inj} = \dot{m}_{inj} C_p T_{01}(\Gamma^{\frac{\gamma-1}{\gamma}} - 1)) \qquad (4.20)$$

Because in the real pump there are losses of various nature like for example, losses due to moving parts that originates frictions, hydraulic losses etc.. it was took in account an efficiency index of the pump defined as $\eta = \frac{P_{id}}{P}$ where P is the total power

requested by the pump. P takes in account all the possible losses and it is assumed that $\eta = 80\%$. At this point it is simply to calculate

$$P = \frac{\dot{m}_{inj} C_p T_{01}}{\eta} (\Gamma^{\frac{\gamma-1}{\gamma}} - 1) \tag{4.21}$$

At this point it is possible to obtain a coefficient similar to the C_L and C_D. In the case of C_L and C_D it is necessary to normalize forces, the Lift and the Drag, that are dependent from the characteristics values of the free stream (ρ_∞, V_∞, etc..). So at the end both C_L an C_D are function constant with the free stream because both the numerator and the denominator are free stream dependent.

$$C_L = \frac{f(V_\infty, \rho_\infty)}{g(V_\infty, \rho_\infty)} \tag{4.22}$$

The numerator of the C_L is the Lift force so at the denominator we should insert some function that has the same dimension of a force. Similarly, in the case of the power, we can start from the power P, expression 4.21and divide it for a function that has the same dimensions of a Power, (Watt in the S.I.) and we will call this ration Power Coefficient, P_c:

$$P_c = \frac{P}{\frac{1}{2} \rho_\infty V_\infty^3 S} \tag{4.23}$$

Chapter 5

Experimental investigations

5.1 Introduction

The experimental P_c was measured starting from Eq. 4.23 and measuring in the Wind Tunnel all the values that appears in the expression. To observe the performance enhancements due to the CFJ, measurements of the C_L and C_D both on the baseline and CFJ airfoil were made. To accurately test the CFJ airfoil, a controlled air delivery system was needed to supply the jet air. This system provides the high pressure air for the injection slot and also employs a vacuum to remove the air from the suction slot. To achieve zero net jet mass flux within the system, the mass flow rates through the injection and suction slots must be equal. It was used a DAS (data acquisition system) to acquire the injection C_μ value so that it could be held constant for each series of tests. Gathering all of the necessary data required a six-component force and moment balance and flow rate sensor equipment, including pressure transducers, thermocouples, orifice plates, and a computer controlled valve. All of this information was compiled in a data acquisition system to be used for each wind tunnel test.

5.2 Wind Tunnel Description

For the experimental investigations it was used a CFJ Wind Tunnel. In the Wind Tunnel facility there are three principal system:

- the Wind tunnel himself;

- the suction line;

- the injection line;

- the Data Acquisition System;

The Wind tunnel mean characteristic mean characteristics are listed here below:

- it is a 24" Open Circuit Wind Tunnel from ERG;

- maximum rotation frequency of the electric motor: 60Hz;
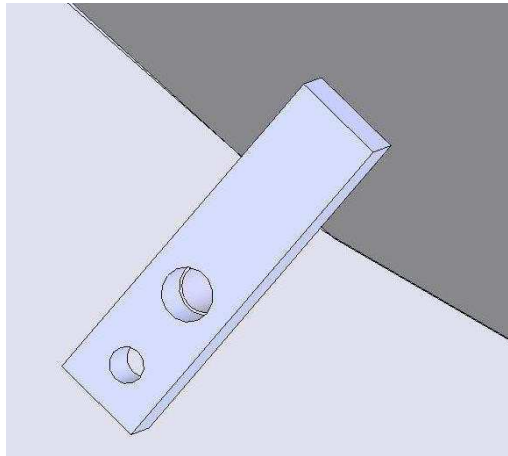
Figure 5.1: Clamp used for securing circular insert
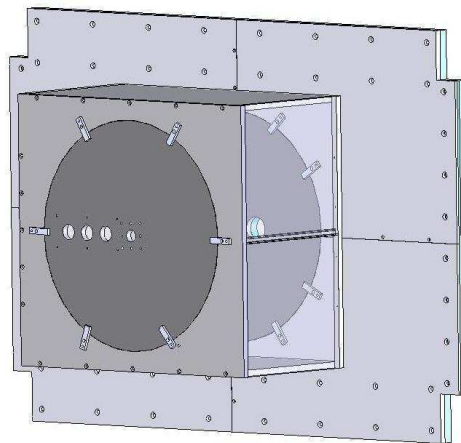
Figure 5.2: Wind Tunnel box

- maximum flow speed in the tunnel: 50 m/s;

- wind tunnel test section:48" $(1.2192\,m)$ long, 24" $(0.6096\,m)$ tall and 24" $(0.6096\,m)$ wide;

- 4 acrylic walls in the test section 0.75" thick reinforced with 0.5" $(1.27\,cm)$ thick aluminum plates;

- the test section is enough large to contain a cambered CFJ airfoil with a 12" $(0.3048\,m)$ chord;

Basically in the test section of the Wind Tunnel, made in plexiglass, it's placed the wing. In the backside of the test section, fig. 5.3 there is a box Fig. 5.2 in which is placed the force-balance 5.4. To change the AoA, was necessary to open the box by screwing the clamps in Fig. 5.1, and to rotate the circular plate that is in contact to the wing.
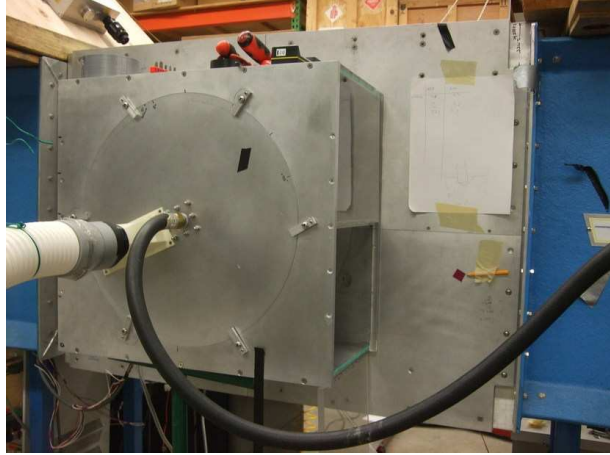
Figure 5.3: Complete Wind Tunnel Box assembly

Figure 5.4: Sting support and force balance

5.3   Air Delivery System

The Wind Tunnel Air Delivery System is needed to provide the Co-Flow Jet airfoil with a high velocity injection jet and to remove air at the suction slot, an air delivery system is necessary. The system was designed to

- maintain a maximum injection $C_\mu = 0.4$ (with a corresponding $\dot{m} = 0.5264$ kg/s) for 60 seconds;

- to remove the air from the suction cavity at the same rate that it entered the injection cavity.

For all the above requirements, the injection line needed:

- a compressor;

- a high pressure air storage tank;

- a computer controlled valve.

The suction side used

- a vacuum pump;

- a vacuum storage tank.

5.3.1   Injection Line

The Injection Line principal components are a compressore and a valve. The main compressor characteristics are:

- it is an Ingersoll Rand UP6-15cTAS-150 compressor;

- it produces 50 CFM (cubic feet per minute) at 150 psi ($0.0236\, m^3/s$ at 1034 kPa);

- it compresses, cools, dries, and then outputs air at $72°F$ ($22.22°C$);

- a 120 gal ($0.4542\, m^3$) air storage tank;

There is an injection air storage tank is 2000 gallons ($7.5708\, m^3$) with a maximum storage pressure of 150 psi. An electro-pneumatic computer controlled valve with feedback control it's used to control the flow into the injection cavity . This valve will be driven by the mass flow rate determined at the orifice plate. If the desired mass flow rate is not matched by the flow meter, the control valve will raise and lower accordingly until the mass flow rate matches the input value at the test stand. The valve is a model IMO-G110-1 and it uses pneumatic force to raise and lower the valve. An amount of air, ranging from $15 - 60$ psi ($103.4 - 413.7$ kPa), is taken from the compressor and an electrical signal, ranging from $4 - 20$ mA, from the computer regulates the air. The reading from the mass flow meter just downstream from the

Figure 5.5: 50 CFM Compressor

Figure 5.6: Pneumatic Computer Controlled Valve
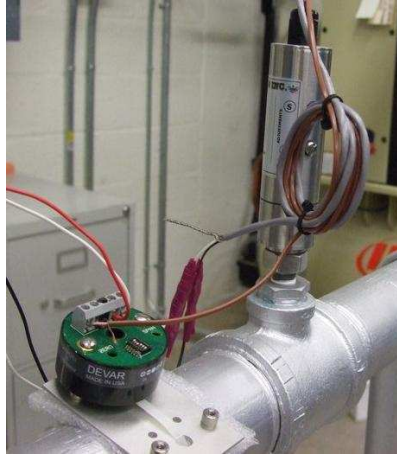
Figure 5.7: Spectre Sensors Model 1500 Pressure/Temperature Transducer

Figure 5.8: Spectre Sensors Model D150 Differential Pressure Transducer

valve tells the valve whether it needs open further or close more. Fig. 5.5 shows the compressor and Fig. 5.6 shows the computer controlled valve used in the CFJ Wind Tunnel Laboratory.

At the exit of the injection tank there is a manual valve that allows the air into the injection line for testing. Various sensor, orifice plates and pressure transducer Fig.5.7 and Fig. 5.8 are placed along the pipeline from the compressor to the wind tunnel to regulate the injection mass flow rate.

Figure 5.9: 60 Hp Vacuum Pump

5.3.2 Suction Line

The suction line is structured as below:

- a 60 hp Dekker V-MAX vacuum pump

- This vacuum pump is connected to a 600 gallon ($2.2712\ m^3$) vertical vacuum tank;

- This tank is used to regulate and maintain a steady vacuum for the suction cavity;

- A gate valve is used to manually adjust the suction flow rate to match the injection mass flow rate;

- A mass flow meter is also located in the suction line between the tank and the suction cavity so that the suction mass flow rate can be determined.

The figure 5.10 shows the entire layout of the Wind tunnel laboratory used during this research.

The piping for the air system is shown in Fig. 5.11.
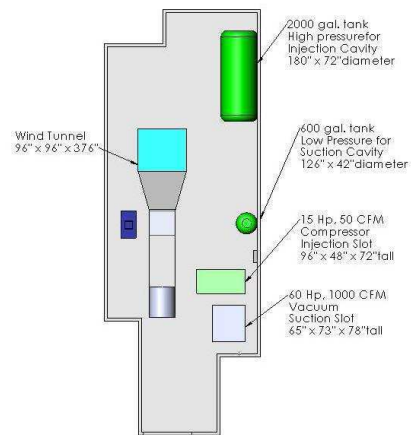
Figure 5.10: Layout of CFJ Wind Tunnel Laboratory

Figure 5.11: Piping for Air Delivery System

Figure 5.12: Overall View of CFJ Wind Tunnel Laboratory

A total pressure pitot probe is located in the suction manifold to measure pressure in the suction cavity. The probe has a 1" (2.54 cm) length and has a 1/8 male NPT fitting for connection to the provided NPT tap in the suction manifold. The outlet of the probe uses clear flexible tube to connect to a barbed hose/female NPT coupler, in the same manner as the pitot probe in the injection cavity. This suction tube connects to a Spectre Sensors Pressure/Temperature Transducer Model 1500 ($0-29.5$" HGV) with a J-type thermocouple. This sensor has a range designed for low pressure vacuum conditions. The T/C wire is not used in the suction cavity.

As the suction air enters the suction cavity from the slot, it travels downstream through the manifold and flexible hoses to the suction line. This pipe has a 3" ($7.62cm$) diameter as it leaves the wind tunnel box and expands to 4" ($10.16cm$) before it reaches the suction line pressure and temperature sensor. Similar to the injection line, the suction line requires a Spectre Sensors Model 1500 Pressure/Temperature Transducer ($0-29.5$" HGV). This sensor also has a male 1/4 NPT that is tapped into the line. This pressure and temperature are used to calculate the suction mass flow rate. The suction line needs a larger 4" Lambda Square Oripac Model 5300 Orifice Plate with connection to a Spectre Sensors Differential Pressure Transducer Model D150 (0-116.9"H2O). This is the same set up as the injection line, just using different range transducers for vacuums.

	Sensor	Reading	Location
1	Electro-pneumatic control valve	Open/Close Valve	Inj. line
2	(0-80 psia) Pres/temp transducer	p_s	Inj. line
3	Temperature transmitter	T	Inj. line
4	(0-267.7" WCD) Differential pressure	Δp	Inj. line
5	(0-80 psia) Pres/Temp transducer	$p_\circ$	Inj. cavity
6	Temperature transmitter	T	Inj. cavity
7	(0-17 psia) Pressure transducer	p_s	Test section
8	MKS Differential pressure	Δp	Test section
9	Thermocouple	T	Test section
10	(0-29.5" HGV) Pres/Temp transducer	$p_\circ$	Suc. cavity
11	(0-29.5" HGV) Pres/Temp transducer	p_s	Suc. line
12	Temperature transmitter	T	Suc. line
13	(0-116.9"H2O) Differential pressure	Δp	Suc. line
14	AMTI force balance	Fx, Fy, Mz	Test section
15	Wind tunnel motor control	Hz of motor	Wind Tunnel

Table 5.1: Sensors and Controls

5.4 Experimental measurement on the Naca6415 baseline profile

Three Mach number for the free stream flow in the wind tunnel were chosen: 0.04, 0.07 and 0.1. For a fixed Mach number, the C_L and the C_D were measured for different AoA in a range that goes from $0°$ to $30°$. Each experimental point was obtained with the procedure below:

- first the wing was mounted on the force balance;

- then the wing was inclined at the good AoA position by manually rotating the exterior circular plate of the test section box;

- both the AoA (that is measured on the sting on the force balance) and the back-plate angle were measured and inserted in *Lab view*;

- all the instrumentation (the Pitot static tube, and the force balance) were initialized;

- the turbine inside the wind tunnel was activated via computer;

- the rotation frequency of the turbine was modified until it was reached the desired Mach number value;

- at this point the record of the data was started;

- all the measured data were automatically recorded on a spreadsheets;

- by using a small Matlab application, all the spreadsheets data were used to create the plots in 5.13:

5.5 Experimental measurement on the Naca6415 CFJ profile

In Chapter 3 it was demonstrated the formula of the power requested from the pump for the CFJ jet :

$$P = \frac{\dot{m_{inj}} C_p T_{01}}{\eta}(\Gamma^{\frac{\gamma-1}{\gamma}} - 1) \tag{5.1}$$

This formula permitted to understand which parameters should be measured to calculate the power P keeping in mind that:

- $\Gamma = P_{01}/P_{02}$;

- P_{01} and P_{02} are respectively the total pressures in the injection and in the suction cavity of the CFJ airfoil profile;

- $c_p = 1003.4 J/Kg/K$;
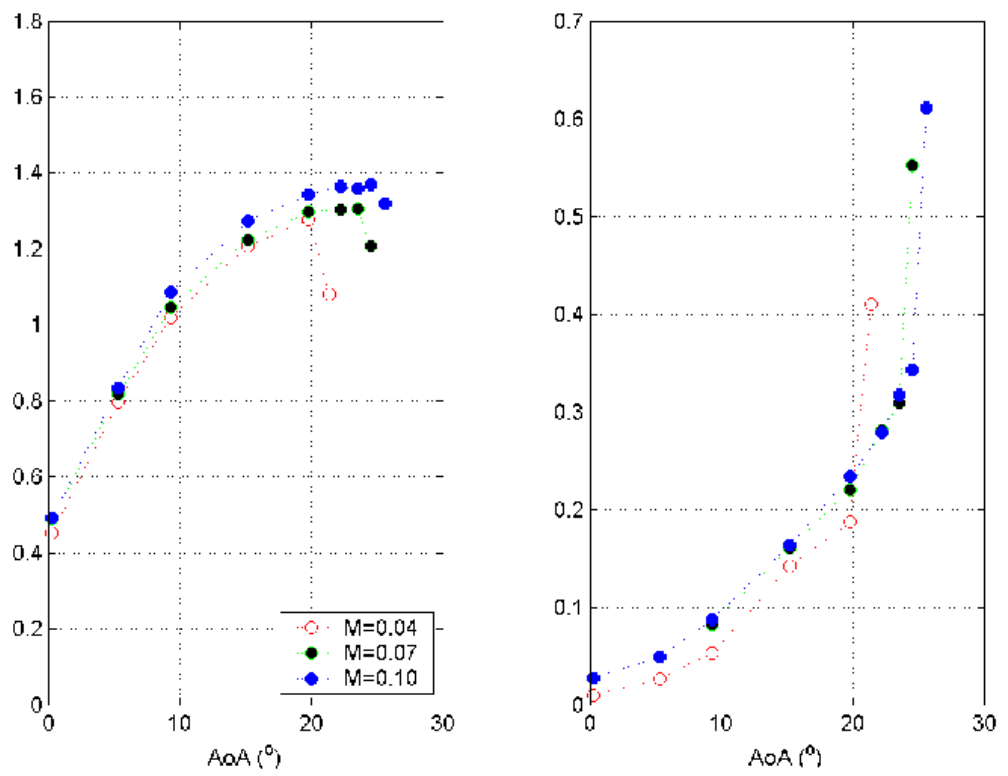
Figure 5.13: NACA6415 experimental C_L and C_D plots
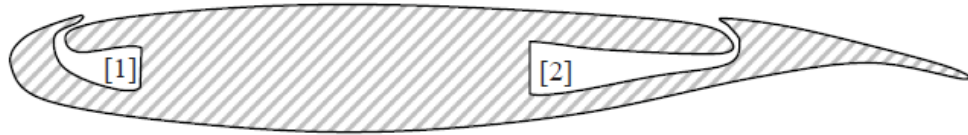
Figure 5.14: Pressure probes locations

- $\gamma = 1.4$ is the ratio of the specific heats for air;

- for the pump efficiency is made the assumption that $\eta_p = 1$ because in the wind-tunnel lab facility the CFJ jet is driven upon a compressor-pipes facility quite different from the true pump that should be used on a real CFJ airfoil;

Different measurement instrument were used to measure the parameters above:

- T_{01}, the injection cavity total temperature, was measured with a thermocouple near the pressure probe location;

- $\dot{m}_{inj}$, the injected mass flow rate, was measured by using $Oripac^{TM}$ orifice mass flow meters equipped with high precision MKS pressure transducers;

- P_{01} and P_{02} , the total pressures, were measured by using some total pressure Pitot probes located respectively in the injection and suction cavities. These probes were connected by a flexible tube to a barbed hose/female NPT coupler. This suction tube connects to a Spectre Sensors Pressure/Temperature Transducer Model 1500.

Figure 5.14 shows the locations where total pressure probes where placed. The pressure measurements were sensibly affected by the position of the probes that should be placed in the correct position respect to the direction of the flow inside the cavities. Because the positioning was very difficult, a measurement of the pressures at the injection and suction slot were done and then also for these values was calculated the power P and was made a comparison with the power P calculated with the true pressure in the cavities.

Each measurement of the power P and so of the power coefficient P_c was made for a particular operating condition establibed by:

- the free stream Mach number;

- the AoA of the wing;

- the C_μ

Once these three parameters were setted up , it wa possible to measure th P_c for that particular case. The free stream Mach number is defined below as :

$$M_\infty = \frac{V_\infty}{\sqrt{\gamma R T_\infty}} \tag{5.2}$$

where R=287.1 J/Kg/K, T_∞ is the room temperature in the wind-tunnel lab facility so it's affected from the actual atmospheric condition of the period in which the experiment is conducted and V_∞ is the magnitude of the free stream velocity and is measured by Pitot tube placed upstream of the wing in the wind tunnel test section. The M_∞ depends on the V_∞ that depends on the rotation frequency of the wind tunnel turbine. So to achieve the correct Mach number this frequency was variated manually via computer using the Labview graphical interface. The C_μ represents the strength of the jet. This parameter is defined as below:

$$C_\mu = \frac{\dot{m} V_{jet}}{\frac{1}{2} \rho_\infty {V_\infty}^2 S} \tag{5.3}$$

and its value derives like the P_c from flow parameters measured in the Wind Tunnel. Once all these parameters were setted up the measurements of P_c was accomplished giving the results on figure 5.15.
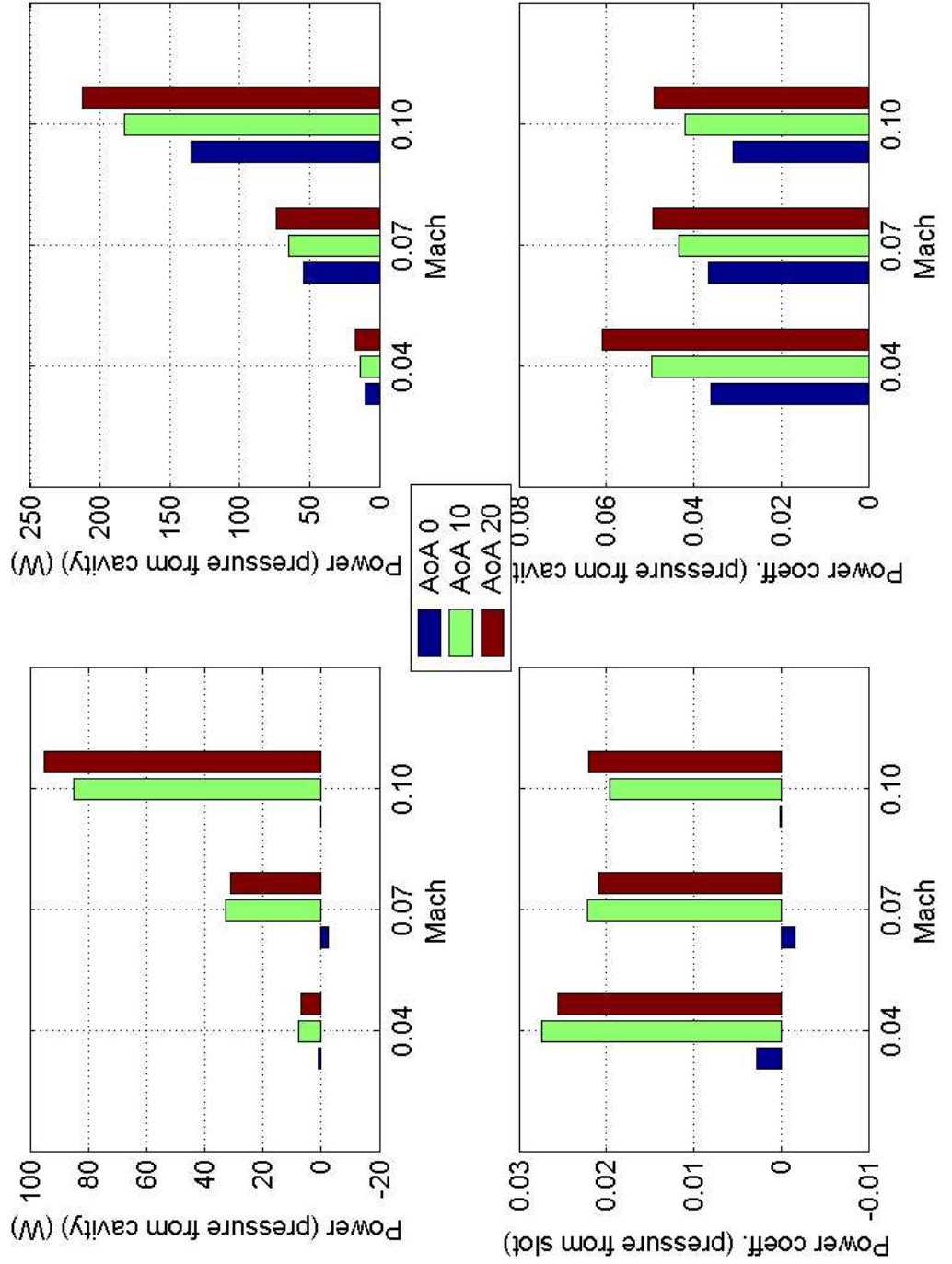
Figure 5.15: Experimental investigation results
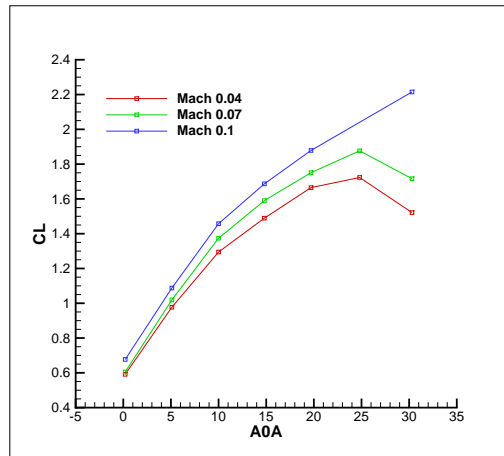
Figure 5.16: Experimental C_L
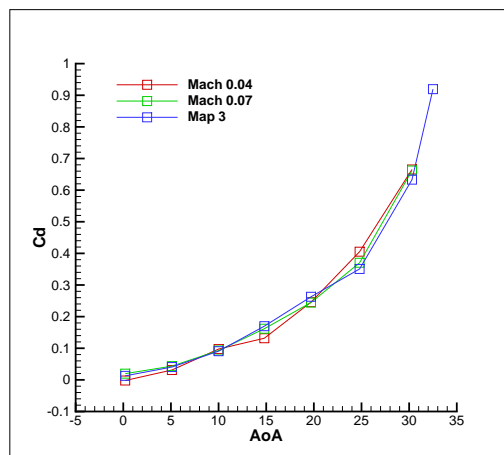
Figure 5.17: Experimental C_D

The experimental results shows that for a fixed value of the AoA, the P_c variations are around at 1% and so are almost negligibles. Then is possible to see that for a fixed Mach number, the P_c increases as the AoA increases. This is due to the fact that as the AoA increases, the back pressure of the wing tends to become higher than the upper pressure (near the leading edge) the results is a negative pressure gradient directed in the opposite direction of the flow around the wing. This gradient is an obstacle for the flow to be attached to the wing surface. At certain point this situation will bring the stall. So the energy requested from the pump to drive the CFJ jet to make to flow attached to the wing surface it will increase. The P_c is defined in the same way of the C_L and C_D, it's a non dimensional coefficient that shows the performances of the CFJ airfoil that unlike the baseline airfoil profile deals with two kind of losses: those related to the Drag force and those related to the energy expenditure of the CFJ system. So it was interesting to study the behavior of *Performance coefficient* defined as $C_L/(C_D + Pc)$ with respect to the AoA. Experimental data about C_L and C_D were taken.
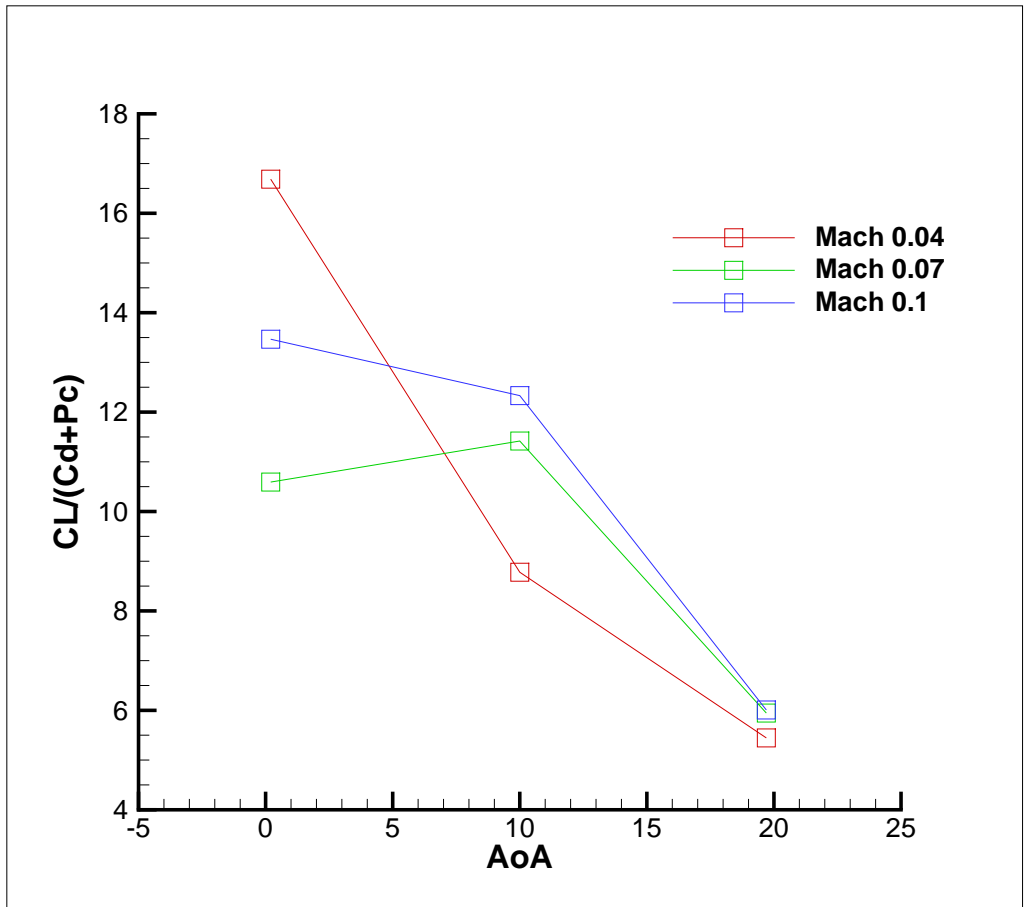
Figure 5.18: Experimental $C_L/(C_D + P_c)$

From figure 5.18 we can observe that the Performance coefficient reduces as the AoA increases accordingly to the fact that the AoA increasing makes growing the C_D therefore as explained above the CFJ pump must work more.

Chapter 6

Numerical investigation

The numerical investigation was conducted using the FASIP (Fluid-Acoustics-Structure Interaction Package) code developed by the CFD-Lab of the University of Miami under the supervision of Dr. Gecheng Zha [29–40]. This code is able to solve numerically non-linear, partial differential Navier-Stokes equations for fluid flow. The code was used to obtain pressure distributions, velocity profiles, streamlines, and non-dimensional aerodynamic coefficients such as C_L, C_D, and C_μ. All results were acquired from 2-dimensional, steady-state simulations of the NACA 6415 baseline airfoil and the CFJ 6415-065-142 airfoil at $C_\mu = 0.05$ and 0.1. The FASIP code required to meshing the flow field, to input the initial conditions and boundary conditions, and to post processing the acquired results. To check the validity of the code, before starting the numerical investigation on the CFJ profile, some benchmark cases were calculated. The CFJ data from the experimental investigation were used to validate the CFJ results obtained from the FASIP code. The Numerical CFJ flow results were obtained by inserting the numerical solution of the Navier Stokes equations into a post-processing code that was developed during this research.

6.1 The numerical investigation procedure

To conduct this numerical investigation on the CFJ airfoil the procedure that was applied is the sequent:

- drawing the CFJ6415 airfoil geometry in Solidworks and exporting it in Gridgenv15;

- modelling the CFJ airfoil mesh using the software Gridgen V15;

- establishing the study case by individuating the AoA, Mach and C_μ;

- normalize the aerodynamics data that should be insert into the datain and init.input files;

- create the init.input using the data related to the mesh blocks;

- insert in the datain all the input data for the calculation;

- launching the FASIP code to obtain the results for the Navier-Stokes equations;

- launching the post processing code to obtain the actual C_μ, P_c, mass flow rates;

- examining the results obtained and eventually re-launch the calculation by modifying the values of the pressures in the injection or suction cavities of the CFJ airfoil.

6.2 Navier-Stokes Equations

Navier Stokes Equations are the governing equations for fluid flow problems. CFD utilizes numerical methods to solve these non-linear partial differential equations. The general 3-dimensional Navier Stokes equation is shown in conservative form in Eq. (6.1).

$$\frac{\partial \mathbf{Q}}{\partial t} + \frac{\partial \mathbf{E}}{\partial x} + \frac{\partial \mathbf{F}}{\partial y} + \frac{\partial \mathbf{G}}{\partial z} = \frac{\partial \mathbf{R}}{\partial x} + \frac{\partial \mathbf{S}}{\partial y} + \frac{\partial \mathbf{T}}{\partial z} \tag{6.1}$$

In the above equation, $\mathbf{Q}$ is the vector of conservative variables; $\mathbf{E}$, $\mathbf{F}$, and $\mathbf{G}$ are the inviscid flux vectors for flux in the x, y, and z directions respectively; and $\mathbf{R}$, $\mathbf{S}$, and $\mathbf{T}$ are the viscous terms.

$$\mathbf{Q} = \begin{pmatrix} \rho \\ \rho u \\ \rho v \\ \rho w \\ \rho e \end{pmatrix} \tag{6.2}$$

$$\mathbf{E} = \begin{pmatrix} \rho u \\ \rho u^2 + p \\ \rho uv \\ \rho uw \\ \rho(\rho e + p)u \end{pmatrix}, \ \mathbf{F} = \begin{pmatrix} \rho v \\ \rho vu \\ \rho v^2 + p \\ \rho vw \\ \rho(\rho e + p)v \end{pmatrix}, \ \mathbf{G} = \begin{pmatrix} \rho w \\ \rho wu \\ \rho wv \\ \rho w^2 + p \\ \rho(\rho e + p)w \end{pmatrix} \tag{6.3}$$

$$\mathbf{R} = \begin{pmatrix} 0 \\ \tau_{xx} \\ \tau_{xy} \\ \tau_{xz} \\ Q_x \end{pmatrix}, \ \mathbf{S} = \begin{pmatrix} \tau_{yx} \\ \tau_{yy} \\ \tau_{yz} \\ Q_y \end{pmatrix}, \ \mathbf{T} = \begin{pmatrix} \tau_{zx} \\ \tau_{zy} \\ \tau_{zz} \\ Q_z \end{pmatrix} \tag{6.4}$$

In these equations, ρ is the density; u, v, and w are the velocity components in the x, y, and z directions respectively; p is the pressure; and e is energy per unit mass. All aspects of fluid flow can be solved from these variables. In Eq. (6.4), the terms Q_x, Q_y, and Q_z are the heat flux terms and are functions of shear stress and velocity components. Eq. (6.5) shows these expanded terms and Eq. (6.6) shows the heat flux in the x, y, and z directions.

$$Q_x = u\tau_{xx} + v\tau_{xy} + w\tau_{xz} - q_x$$
$$Q_y = u\tau_{xy} + v\tau_{yy} + w\tau_{yz} - q_y \qquad (6.5)$$
$$Q_z = u\tau_{xz} + v\tau_{yz} + w\tau_{zz} - q_z$$

$$q_x = -\frac{\mu}{(\gamma-1)Pr}\frac{\partial a^2}{\partial x}$$
$$q_y = -\frac{\mu}{(\gamma-1)Pr}\frac{\partial a^2}{\partial y} \qquad (6.6)$$
$$q_z = -\frac{\mu}{(\gamma-1)Pr}\frac{\partial a^2}{\partial z}$$

In the above equation, Pr is the Prandtl number and is defined as follows where ν is kinematic viscosity, α is the thermal diffusivity in this case, and γ is the ratio of specific heats.

$$Pr = \frac{\nu}{\alpha} \qquad (6.7)$$

The viscous shear stress terms from Eq. (6.5) are shown as follows.

$$\tau_{xx} = \tfrac{2}{3}\mu\left(2\frac{\partial u}{\partial x} - \frac{\partial v}{\partial y} - \frac{\partial w}{\partial z}\right)$$
$$\tau_{yy} = \tfrac{2}{3}\mu\left(2\frac{\partial v}{\partial y} - \frac{\partial u}{\partial x} - \frac{\partial w}{\partial z}\right)$$
$$\tau_{zz} = \tfrac{2}{3}\mu\left(2\frac{\partial w}{\partial z} - \frac{\partial u}{\partial x} - \frac{\partial v}{\partial z}\right)$$
$$\tau_{xy} = \tau_{yz} = \mu\left(\frac{\partial u}{\partial y} - \frac{\partial v}{\partial x}\right) \qquad (6.8)$$
$$\tau_{xz} = \tau_{zx} = \mu\left(\frac{\partial w}{\partial x} - \frac{\partial u}{\partial z}\right)$$
$$\tau_{yz} = \tau_{zy} = \mu\left(\frac{\partial v}{\partial z} - \frac{\partial w}{\partial y}\right)$$

The first terms in Eq. (6.2), (6.3), and (6.4) form the Continuity Equation, or conservation of mass. The 2nd through 4th terms make up the u, v, and w directions of the Momentum Equation. Finally, the 5th term makes up the Energy Equation. All of these equations together can be solved simultaneously using various differencing schemes by CFD. From this, the density, velocity in three directions, pressure, and energy can be found at every point within the discretized space.

Turbulence modeling of fluid flow is very complex and much work has been done in the field to accurately capture this chaotic and seemingly unsolvable phenomenon. However, there are many approximation methods that are shown to have accurate results. These turbulence models include algebraic solving, one-equation, two-equation, Large Eddy Simulation (LES), Direct-Eddy Simulation (DES), and Direct Numerical Simulation (DNS) [45–47]. The FASIP CFD code is equipped with solvers for the algebraic Baldwin-Lomax (BL) model, the one-equation Spalart-Allmaras (SA) model, LES, and DES. For this work, the BL turbulence model is used with Reynolds averaged Navier-Stokes equations for their robustness and high CPU efficiency. This model is often used when the turbulent boundary layer is very thin compared to the overall geometry and the discretized cell size along the wall is small. Such applications include the aerodynamic modeling of wings.

6.3 The normalization of fluid-dynamics parameters

All the fluid-dynamic parameters involved in the calculations were normalized before to be inserted in the FASIP code this for two main reasons:

- to create a similar solution;

- to reduce the round-off error due to the computer;

For this research was necessary to normalize the fluid-dynamic parameters (p, T, μ, u, v, w, e) by using the fluid-dynamic parameters of the free-stream (∞) and the characteristic dimensions of the CFJ airfoil profile ($lref = wingchord$, $s = wingspan$). Finally was necessary to express the aerodynamics coefficients (C_L, C_D and C_μ) in function of the non dimensional parameters because the code uses only these ones.

6.3.1 Fluid-dynamic paramenters normalization

The normalized fluid-dynamic paramenters are:

$$\bar{\rho} = \frac{\rho}{\rho_\infty} \tag{6.9}$$

$$\bar{u} = \frac{u}{u_\infty} \tag{6.10}$$

$$\bar{v} = \frac{v}{v_\infty} \tag{6.11}$$

$$\bar{w} = \frac{w}{w_\infty} \tag{6.12}$$

$$\bar{T} = \frac{T}{T_\infty} \tag{6.13}$$

$$\bar{x} = \frac{x}{L_\infty} \tag{6.14}$$

$$\bar{y} = \frac{y}{L_\infty} \tag{6.15}$$

$$\bar{z} = \frac{z}{L_\infty} \tag{6.16}$$

$$\bar{e} = \frac{e}{V_\infty^2} \tag{6.17}$$

$$\bar{p} = \frac{p}{\rho_\infty V_\infty^2} \tag{6.18}$$

$$\bar{\mu} = \frac{\mu}{\mu_\infty} \tag{6.19}$$

$$\bar{t} = \frac{t}{L_{ref}/V_\infty} \tag{6.20}$$

6.3.2 Fluid-dynamic equations normalization

The Navier Stokes equations need to be normalized to be calculated from the FASIP code. The solution of those normalized is:

$$\bar{q} = \frac{q}{\mu_\infty V_\infty^2 / L_{ref}} \tag{6.21}$$

$$\bar{\tau} = \frac{\tau}{\mu_\infty V_\infty / L_{ref}} \tag{6.22}$$

The Navier-Stokes equations normalized become:

$$\frac{\partial \bar{\mathbf{Q}}}{\partial \bar{t}} + \frac{\partial \bar{\mathbf{E}}}{\partial \bar{x}} + \frac{\partial \bar{\mathbf{F}}}{\partial \bar{y}} + \frac{\partial \bar{\mathbf{G}}}{\partial \bar{z}} = \frac{1}{Re} \frac{\partial \bar{\mathbf{R}}}{\partial \bar{x}} + \frac{\partial \bar{\mathbf{S}}}{\partial \bar{y}} + \frac{\partial \bar{\mathbf{T}}}{\partial \bar{z}} \tag{6.23}$$

The Reynolds number itself is defined as a non-dimensional parameter:

$$R_e = \frac{\rho_\infty L_{ref} V_\infty}{\mu_\infty} \tag{6.24}$$

The equation that states the law of perfect gas is

$$p = \rho R T \tag{6.25}$$

and after normalization it becomes:

$$\bar{p} = \frac{1}{\gamma M_\infty^2} \bar{\rho} \bar{T} \tag{6.26}$$

Finally in the post processing code is useful the normalized formula that relate the specific energy e of the flow to the pressure and to teh velocity field:

$$\bar{\rho} e = \frac{\bar{p}}{\gamma - 1} + \frac{1}{2} \bar{\rho}(\bar{u}^2 + \bar{v}^2 + \bar{w}^2) \tag{6.27}$$

6.3.3 Normalization of C_L, C_D, C_μ and P_c

C_L and C_D are both related to the pressure distribution around the wing and their formula in the code is referred to only a segment between two consecutive cells that describe a surface. In the case of C_L, this coefficient is for definition the Lift force, L, normalized by using the dynamic pressure force of the free stream at the denominator:
NB:$l_r ef$ is the airfoil chord c, s=airfoil span

$$C_L = \frac{L}{\frac{1}{2}\rho_\infty V_\infty^2 cs} \tag{6.28}$$

$$L = ps L_w \tag{6.29}$$

L_w is the perimeter lenght of the profile of the wing in a plane normal to the airfoil span direction; by substituting the 6.29 in the 6.28 and after some passages we obtain:

$$C_L = 2\frac{p}{\rho_\infty V_\infty^2}\frac{L_w}{c} \tag{6.30}$$

The ratios that appear in the previous formula are non dimensional parameters:

$$C_L = 2\bar{p}\bar{L}_w \tag{6.31}$$

In similar way C_D can be obtained. C_μ is defined as:

$$C_\mu = \frac{\dot{m}_{inj}V_{inj}}{\frac{1}{2}\rho_\infty V_\infty^2 cs} \tag{6.32}$$

It's necessary to introduce the non dimensional mass flow-rate:

$$\bar{\dot{m}}_{inj} = \frac{\dot{m}}{\rho_\infty V_\infty c^2} \tag{6.33}$$

The non dimensional injection jet velocity of the jet is

$$\bar{V}_{inj} = V_{inj}/V_\infty \tag{6.34}$$

By using 6.33 and 6.34 in the definition of C_μ it's possible to obtain:

$$C_\mu = 2\bar{\dot{m}}_{inj}\bar{V}_{inj}\frac{c}{s} \tag{6.35}$$

If in the 6.33 the dimensional mass flow rate is explicitated in function of the *injection slot area* that is the product of the injection slot height h_{inj} and the span s it's possible to obtain:

$$\bar{\dot{m}}_{inj} = \frac{\rho V_{inj}h_{inj}s}{\rho_\infty V_\infty c^2} \tag{6.36}$$

in the latest expression, all the ratios are non-dimensional parameters:

$$\bar{\dot{m}}_{inj} = \bar{\rho}\bar{V}_{inj}\bar{h} \tag{6.37}$$

finally substituting the 6.37 in the 6.35 it's possible to obtain:

$$C_\mu = 2\bar{\rho}\bar{V}_{inj}^2\bar{h} \tag{6.38}$$

The formula 6.38 it's used in the code. The last parameter that was normalized was the P_c. By combining the definitions 4.21 and 4.23 it's possible to obtain:

$$P_c = \frac{\dot{m}_{inj}c_pT_{01}}{\frac{1}{2}\rho_\infty V_\infty^3 sc}(\Gamma^{\frac{\gamma-1}{\gamma}} - 1) \tag{6.39}$$

it's necessary to introduce the non-dimensional air specific heat at constant pressure:

$$\bar{c}_p = c_p\frac{T_\infty}{V_\infty^2} = \frac{1}{M_\infty^2(\gamma - 1)} \tag{6.40}$$

The combination of the formulas 6.37, 6.40 and 6.39 bring to:

$$P_c = \frac{c}{s}\frac{\bar{\dot{m}}\bar{T}_{01}}{M_\infty^2(\gamma - 1)}(\Gamma^{\frac{\gamma-1}{\gamma}} - 1) \tag{6.41}$$

6.4 Technical data about the computers used for the numerical investigations

The first study cases were used to test the code and to find eventually errors. The mesh was modified respect to the original model, and was also launched a 3-dimensional model, etc.. All this works required to use super-computers. The ones available for this research were the CFD-lab at University of Miami were:

- **Ydpa**: it has 108 Intel Core 2 5150, each one is dual core, so in total 216 CPU.;the total memory is $54 server * 4 = 216 Gbytes$. Times ago, the YDPA performance was tested with all the CPU working on parallel; in this condition Ydpa achieves 1 Teraflop which means 1000Gigaflop for scientific calculations;

- **Mars**: this is the oldest one with 56 Pentium Xeon 2.8Ghz CPU, each ones includes hyperthreading so the total that appears is 112CPU but the hyperthreading doesn't double the performance. Usually 1CPU with hyperthreading appears like 2 CPU but it gives the same performance of 1.5 CPU. In comparison with YDPA, Mars performance can be estimated like this: $56*1.5 = 84CPU$ that are equivalent to $84/2 = 42$ CPU of YDPA. (the speed one CPU of Mars is equivalent to an half of the speed of a CPU of YDPA) so $1000/216 = 4.6$ Gigaflop for YDPA. So Mars can reach $1000/216 = 4.6 Gigaflop$ and YDPA can reach $CPU * 42 = 200$ Gigaflop;

- **Pegasus**:is a blade based cluster available for M/EPP (Massive/Embarrassingly Parallel) simulations and data analysis tasks. The cluster consists of over 1,000 compute nodes. These nodes are interconnected within their enclosures by Gigabit Ethernet and outside their enclosures with 10 Gigabit Ethernet. The cluster also features a 35 TB High Performance File System, for maximum performance of both parallel and serial access. This system provides an aggregate 5,230 Intel Xeon Cores and 7.4 TB of aggregated memory. These systems are configured to provide a development and job running environment similar to those that are available in other HPC centers.

6.5 General notions about the mesh

The FASIP code uses implicit schemes, which are unconditionally stable and can be proved so via Von Neumann analysis. This means that the unknowns exist in time step $n + 1$ and they are solved simultaneously for every solution point in that time step [47]. For the FASIP are availables several differencing schemes that can be applied to the equations for different orders. The higher the order of the equation, the more accurate the results will be because the truncation error is reduced when more terms are included in the calculations. For each case of simulations for the baseline

Figure 6.1: The YDPA parallel computing system

Figure 6.2: The High Power Calculation center where Pegasus is located

and CFJ airfoil the same schemes and orders are used. The Zha3 Low Diffusion E-CUSP (Convective Upwind and Split Pressure) scheme is used for the right hand side (RHS) of the interface equation [35,36,40,45,46]. This scheme utilizes vector splitting of the inviscid flux terms into convective and pressure parts. For this scheme, the inviscid fluxes were evaluated using 3rd order accuracy. The viscous terms are found using 2nd order central differencing. The Van Leer Scheme was used to evaluate the implicit left hand side (LHS) with a 1st order MUSCL scheme (Monotone Upstream-Centered Schemes for Conservation Laws) to enhance diagonal dominance.

The real CFJ-6415 mesh was modeled in the virtual environment of the computer by a meshing process. It's important to specify that:

- respect to the real case the mesh-model is made in 2 dimensions;

- not all the components of the the true CFJ airfoil were (like the aluminum foam, etc) were modeled into the mesh'

For the purposes of the numerical investigation, the control volume around the wing was modeled and meshed because the FASIP code work by solving a discrete representation of the Navier-Stokes equations on each cell center of the mesh. Sometimes the space will contain the geometry of a solid body that will interact with the flow. For this research, the free stream flow field contains baseline and CFJ airfoils. The modeled space is the control volume. It can be simply-connected if it can be reduced to a single point or it can be doubly-connected [46] if there is a geometry enclosed within the mesh and the space is not reducible.

For this work, the cell shape chosen is rectangular. For 2-dimensional meshing each cell has 4 node points at the corners and for 3-dimensional meshes each cell has eight node points. The CFD simulation performed on the NACA 6415 baseline and the CFJ 6415-065-142 airfoils is 2-dimensional. Since the solution points are found from a finite volume method at the center of each cell, the accuracy of the results are dependent on the size of each mesh cell.

The finer is mesh the higher will be the accuracy but the CPU time will also increase . This is a trade off that varies with each case and depending on the type of results required. In general,the mesh should be finer in the case of a large flow gradient with more complex flow interaction and higher turbulence. So, the mesh size at wall boundaries is much finer than further out in the flow field. It's necessary to obtain aerodynamic force coefficients, pressure distributions and velocities near the airfoil surface.

For very big mesh, CPU time can be reduced by splitting the mesh into sections and running them simultaneously using an MPI (Message Passing Interface) parallel computing process. This is one main characteristics of the way in which the FASIP code works [31]. For all the reasons during the mesh creation process, the height of the cells on the airfoil surface (the wall) also called $y+$ was eximated by the formula 6.42.

$$y+ = \frac{u_* y}{\nu} \tag{6.42}$$

where:

- u_* is the is the friction velocity at the nearest wall;

- y is the distance to the nearest wall;

- ν is the local kinematic viscosity of the fluid.

NB: dimensional analysis shows that at a wall a charateristic velocity, called the friction velocity, can be defined in the following way :

$$u_* = \sqrt{\frac{\tau_w}{\rho}} \tag{6.43}$$

Where τ_w is the wall shear stress and ρ is the fluid density at the wall.

The mesh is grid of point that should fit the geometry of the CFJ-6415 airfoil that is a complicated geometry. Each grid point is a node that is assigned a real coordinate in Cartesian space. This is called the physical domain and has values for each x, y, and z coordinate. This domain needs to be transformed into a rectangular shape for CFD analysis and this is called the computational domain with coordinates ξ, η, and ζ [46]. This allows the original physical domain with more complex shapes to align with the computational domain's rectangular axis. The FASIP code includes an executable that converts the physical domain into the computational domain.

The structured physical mesh required by the FASIP CFD code used in this research was generated using the software Gridgen Version 15.
The airfoil geometry produced was converted to an *.iges* file and imported into Gridgen as data points. This process was done for both the baseline and CFJ airfoils. The flow field was modeled around the airfoils in the far field and in the interior injection and section cavities for the CFJ airfoil. With the model loaded into Gridgen, all non-essential lines from cuts and extrusions were removed in preparation for the flow field meshing. Then the far field was generated with one-dimensional segments called connectors. The baseline and CFJ airfoils were created the same way, except that the baseline did not have interior cavities or the lowered suction surface. Once the segments were created, each one was dimensioned with a certain number of points from which each node of the mesh would be created. Also, the distribution of these points was assigned as well with the smaller distribution near the walls where boundary layers would exist. Then, 2-dimensional domains were created and bounded by 4 connectors. The dimensions of each opposite connector within the domain needed to have the same number of points.

6.6 The Naca6415 baseline airfoil profile

6.6.1 Introduction

In this section it will be explained how was modeled the Naca6415 starting from the mesh process and arriving to the necessary data that were inserted into the input files (datain and init.input) used by the FASIP code to start the calculations.
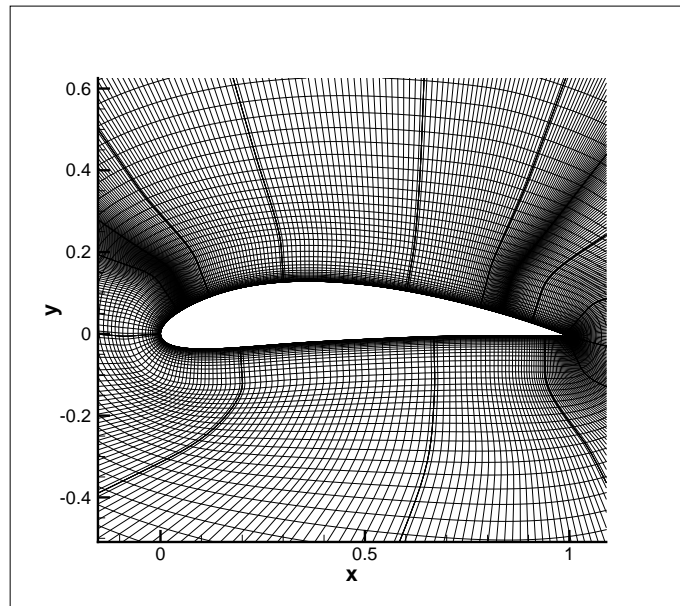
Figure 6.3: NACA6415 baseline airfoil profile mesh

6.6.2   Step 1: The mesh

Once the geometry was imported into Gridgen the mesh , so the 2-dimensional grid, was generated. For all the reasons explained above the mesh was divided into domains, it was made coarse in the far-field and finer near the wing surface by estimating the $y+$. Because of the complicated geometry of the wing, once the mesh is created, many cells, specially the ones near the wing surface were very deformed, so to make the more squared and so to improve the quality of the mesh, it was launched a mesh solver to refine the mesh. The original mesh has AoA 0 and for each other case, which means for each other AoA, the mesh was rotated in Gridgen.

Because all the study cases are in 2-dimension we will speak in terms of domains that represent surfaces instead of blocks, these latter are used in the 3-dimensional case because they represents volumes The whole control volume is modeled by an o-mesh which is basically a grid with radial and circumferential directions (this latter cause the mesh called o-mesh).

Fig. 6.3 shows the the baseline airfoil. The domains have same number of nodes.

The domains dimensions for the baseline airfoil meshes are given in tables 6.1. These values are the number of cells along each connector in the ξ, η, and ζ direction. If the total number of node points in each connector is l than the number of cells along that particular connector is $l-1$. The mesh is 2-dimensional so along ζ there are zero connectors. There are totally 15 domains all around the airfoil profile.

When building the mesh in Gridgen, the number of node points is specified for each connector. However, when setting up boundary and initial conditions in the FASIP code, the number of cells is given. For each domain, the node points are first set to have equal distances between each, then the cell size is specified and redistributed at the surface of the airfoil and the walls. This is input as $\Delta y = 0.003$.

Block	ξ-Direction	η-Direction	ζ-Direction	Total Nodes
1	31	101	0	3131
2	31	101	0	3131
3	31	101	0	3131
4	31	101	0	3131
5	31	101	0	3131
6	31	101	0	3131
7	31	101	0	3131
8	31	101	0	3131
9	31	101	0	3131
10	31	101	0	3131
11	31	101	0	3131
12	31	101	0	3131
13	31	101	0	3131
14	31	101	0	3131
15	31	101	0	3131
total	-	-	-	46965

Table 6.1: Block Allocation for Naca6415 baseline airfoil

The final result was a file.grd that is a file that contain the whole grid that represents the mesh of the entire control volume of the airfoil profile. The file is the list of the grid nodes coordinates. The grid is made by nodes, and 4 nodes are the corner points of a single cell. A single cell is a square and its center is called *cell-center*. During the meshing process it was attempt to obtain domains with same dimension in the same directions. This because when the MPI boundary conditions will be written it will be more easy to specify the coordinates of the border line within two adjacent domains. This concept will be discussed in one of the next sections.

6.6.3 Step 2: creating the domains input file

Once the file.grd was obtained,his name was changed in geo.grd to make the file capable to be elaborated by a Fortran application, the *Plot3d2rans*. This is a program developed in the CFD-lab at University of Miami, under the supervision of Dr.Gecheng Zha. This program read in input the geo.grd and produces a number of bin-file.dat equal to the domains number. For instance in the case of the Naca6415 the output will be a group of 15 files as below:

- bin2d_001.dat

- bin2d_002.dat

- ....

- ....

- bin2d_015.dat

Each one of this file represents a domain that will be calculated from a single processor, called node, of a super- computer.

6.6.4   Step 3: inserting the domains data in the init.input file

Part of the input data used by the FASIP code to start the calculation is contained in a text file called *init.input*. This file contains all the informations related to the domains:

- total number of the domains;

- dimensions of each domains;

- eventually additional initial conditions, such for example in the case of the CFJ6415 profile the values of the total pressure and temperature in the injection cavity, and static pressure in the suction cavity.

Here below is shown the *init.input* file used for the baseline calculations:

```
200, 0      !bc_max  the maximum of the BCs number defined in problem
15          !nb  the total number of blocks
30,100,1    !il,jl,kl  the cell's dimension of the grid of each block
30,100,1    !il,jl,kl  the cell's dimension of the grid of each block
30,100,1    !il,jl,kl  the cell's dimension of the grid of each block
30,100,1    !il,jl,kl  the cell's dimension of the grid of each block
30,100,1    !il,jl,kl  the cell's dimension of the grid of each block
30,100,1    !il,jl,kl  the cell's dimension of the grid of each block
30,100,1    !il,jl,kl  the cell's dimension of the grid of each block
30,100,1    !il,jl,kl  the cell's dimension of the grid of each block
30,100,1    !il,jl,kl  the cell's dimension of the grid of each block
30,100,1    !il,jl,kl  the cell's dimension of the grid of each block
30,100,1    !il,jl,kl  the cell's dimension of the grid of each block
30,100,1    !il,jl,kl  the cell's dimension of the grid of each block
30,100,1    !il,jl,kl  the cell's dimension of the grid of each block
30,100,1    !il,jl,kl  the cell's dimension of the grid of each block
30,100,1    !il,jl,kl  the cell's dimension of the grid of each block
0
```

It's necessary to pay attention to the fact that while in the Gridgend the grid is made by considering the nodes, the FASIP code works on the cell centers. So the dimension of the domain expressed in terms of cell center is equal to the dimension expressed in terms of nodes minus 1. So it's possible to see that the dimension of a single domain in the init.input file are expressed in cell center: $300, 100$ while the same dimensions in the table 6.1 are increased by 1 because they are expressed in terms of nodes.

6.6.5 Step 4: inserting the initial and boundary (BC) conditions in the datain file

Into the datain file they were inserted two kind of data:

- the *initial conditions* that are the initial values of the fluid-dynamics parameters (Mach, temperature, density,etc,..) due to the free-stream;

- the *boundary conditions*(BC) that specify the kind of boundary at each border line of each domain.

- the scheme selection data and CFL.

The FASIP code works on non-dimensional values, so all the initial conditions fluid-dynamics data, were normalized according to Chapter 5, section 5.3, and then inserted into the datain. Initial values are given for the pressures and temperatures for the incoming free stream flow. Reynolds number is also given as a flow parameter and is shown in Eq. (6.44).

$$Re = \frac{\rho U L}{\mu} \tag{6.44}$$

The free stream density, velocity, and viscosity are used in this equation. The reference length (L) is the chord length of the airfoil. Reynolds number comes from normalization of the Navier-Stokes equations given in Eq. (6.1). In the study case of a baseline airfoil profile with a free stream Mach number of 0.03 to be inserted into the datain are shown in the table 6.2:

Variable	Value
Mach	0.03
p_{outlet}	793.650794
p_{total}	794.150906
Reynolds	208361.77
T_{total}	1.00018
T_{ref}	0.377054

Table 6.2: Normalized Initial Conditions for FASIP *datain* file

Here, p_{outlet} is the static pressure of the free stream flow, p_{total} is the total pressure of the free stream, T_{total} is the total temperature, and T_{ref} is a reference temperature used to by the code to calculate free stream viscosity from Sutherland's Law. All of the above values, with the exception of T_{ref} and Re, can be found from the Mach number given for the simulations. These relations are given in Eq. (6.45), (6.46), and (6.47).

$$p_{outlet} = \frac{1}{\gamma M^2} \tag{6.45}$$

$$\bar{p}_{total} = \frac{p_{total}}{p_\infty} \left(1 + \frac{\gamma - 1}{2} M^2 \right)^{\frac{\gamma}{\gamma - 1}} \tag{6.46}$$

$$\bar{T}_{total} = \frac{T_{total}}{T_\infty} \left(1 + \frac{\gamma - 1}{2} M^2 \right) \tag{6.47}$$

The Reynolds number shown in table 6.2 was found using standard values for density, velocity at $Mach = 0.03$, and viscosity. The reference length used here is the chord length of both airfoils, 12 in. or 0.3048 m. Data from wind tunnel testing for the free stream total pressure, static pressure, total temperature, and velocity was used to determine the non-dimensional inputs for the `datain` file. The data fluctuated slightly for each angle of attack test with the baseline and CFJ airfoils. Since the wind tunnel data is dimensional, the values in Table 6.3 for p_{outlet}, p_{total}, T_{total}, and T_{ref} are normalized. These dimensional values were found using a Pitot tube and a thermocouple in the wind tunnel test section. Since the thermocouple measures the temperature directly in the wind tunnel when the free stream was moving and , the value for T_{total} was normalized by itself and resulted in $T_{total} = 1.000$ for all angles of attack. The equation for T_{ref} is as follows and this value utilizes T_∞ being the free stream temperature found by the thermocouple. This input is then used by the code to calculate viscosity. The values used are in Kelvin.

$$T_{ref} = \frac{110.4}{T_\infty} \tag{6.48}$$

Values for total and static pressures were found from the wind tunnel data. The equation normalizing any pressure for p_{outlet} and p_{total} is as follows. The density also comes from the wind tunnel data.

$$\bar{p} = \frac{p}{\rho_\infty V_\infty^2} \tag{6.49}$$

Previous data, table 6.3 [43] for Mach 0.1, show that the dimensional initial condition measured in the wind-tunnel slightly variate as the AoA variates. This is due to the acceleration effect on the free-stream due to the curvature induced by the wing. Because the flow is subsonic, each perturbation is propagated in all the directions and this affects the measurement obtained by the thermocouple and the Pitot tube in the proximity of the wing.

Since the FASIP code is equipped with several differencing schemes at various orders of accuracy and multiple turbulence models, the schemes used for each CFD simulation must also be included in the initial inputs. This information is provided in the `datain` file. Table 6.4 shows the schemes chosen for all cases for both baseline and CFJ airfoil simulations. The CFL (Courant-Friedrichs & Lewy) number is included as well, and it is described in Eq. (6.50).

$$CFL = \frac{c \Delta t}{\Delta x} \tag{6.50}$$

α	Mach	p_{outlet}	p_{total}	Re	T_{total}	T_{ref}
0	0.1	71.4683	71.9684	667950	1.000	0.37077
5	0.1	71.4711	71.9713	666057	1.000	0.37073
10	0.1	72.2193	72.7194	661755	1.000	0.37007
15	0.1	71.3405	71.8406	664985	1.000	0.36977
18	0.1	71.3768	71.8770	665308	1.000	0.37001
20	0.1	71.3768	71.8770	665308	1.000	0.37001

Table 6.3: Final Inputs for Baseline

Variable	Value
CFL	10
LHS Scheme	Van Leer
LHS Order	1st Order MUSCL
RHS Scheme	Zha3
RHS Order	3
Turbulence Model	Baldwin Lomax

Table 6.4: Scheme Selection for Baseline and CFJ Simulations

Along with initial conditions, the code also requires boundary conditions for the fluid flow domain. FASIP makes use of several types of boundary conditions for various cases. For the baseline and CFJ airfoil cases, boundaries are defined at all faces of each mesh block. The following boundary conditions are used for the baseline case.

- BC 3 - no-slip adiabatic wall boundary given at all airfoil surfaces and mesh sides where $\zeta = 1$ and $\zeta = Max$

- BC 5 - subsonic outflow, fixed static pressure for suction cavity

- BC 6 - subsonic inflow used at the far-field where flow is entering the region

- BC 7 - interface boundary for MPI used at all subdomain boundaries for parallel computing

For the CFJ case, the above conditions are used along with these addition boundary conditions to define the flow going into the injection cavity and out of the suction cavity.

- BC 9 - subsonic inflow with total pressure specified, used for incoming flow in injection cavity

Figure 6.4shows the different domains in which the baseline airfoil is divided. The two points, A and B represents the borders between the far field inlet flow (BC 6) and far field outlet flow (BC 5 and not 11 in our case).
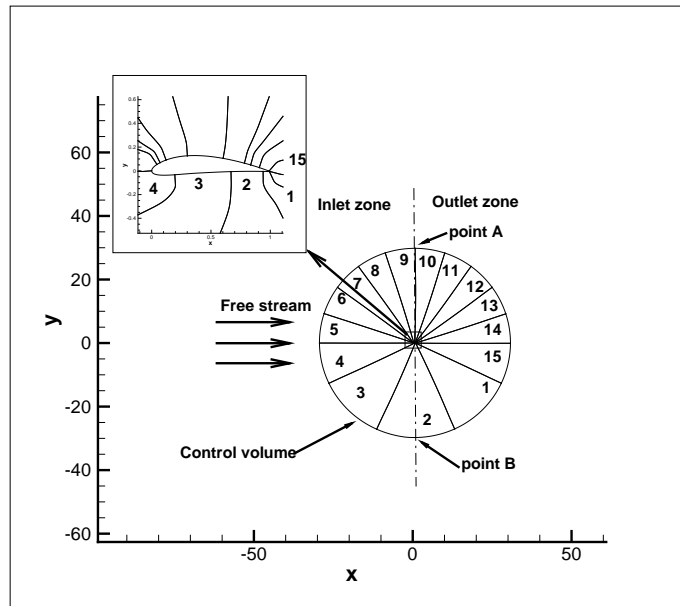
Figure 6.4: Baseline domains geometry and boundary conditions rapresentation

the BC are used to simulate different boundary on which the domains border are contact, for instance:

- BC 3 represent the contact between the flow and the surface of the wing: because there is the friction effect, at the wall the flow velocity is zero; this BC is defined along the airfoil surface where the coordinate $\eta = 1$;

- BC 5 is defined along the side of the suction cavity. This BC simulates how the flow will be removed from the side of the airfoil during wind tunnel testing. BC 5 is also used to simulate the outflow in the far field;

- BC 6 represents the free stream flow approaching the control volume region in the far field with respect to the airfoil;

- BC 7 represents the fact that 2 adjacent domains are in contact each other along a border line which coordinates are specified in the BC7 in both the local reference frame of each of the two domains; each domain is calculated in a single computer processor and then the informations about the two domains are exchanged along the border surface thanks to the BC 7 that physically asks to the 2 computer processor to make this information exchange. This border line represents an open M.P.I. (message passing interface);

- BC 9 enters along the span of the injection cavity with $\xi = 1$ with a given total pressure. This will also simulate the wind tunnel test as the uniform flow entering the injection cavity after the aluminum foam. Total pressure in the injection cavity and static pressure in the suction cavity can be adjusted for the each CFD case to control and maintain equal mass flow rates exiting and entering the cavities.

These boundary conditions are assigned to each mesh surface via cell number. For each change in α, the airfoil is rotated within the mesh and the boundary conditions for far field inflow and outflow are adjusted as well.

6.6.6 Step 5: fixing the study cases and launching the calculations

For the baseline profile it was needed to calculate the C_L and C_D for AoA:0°, 5°,10°, 15° and 20°. Because both the coefficients are independent from the free-stream flow conditions and so from the Mach number, all these calculations where made for Mach 0.03. These study cases where calculated using some super computers:

- YDPA;

- Mars;

- Pegasus.

The procedure for launching a single calculation for one study case is:

- setup datain and init.input;

- launching init.out: this application receives in input the input data from datain and init.input and it writes the *rstart* files that are the initial conditions that can be read from the main.out

- allocating in the super computers a number of processors equal to the number of the domains involved in the study case;

- launching the main.out

- stopping the calculation when the solution converges;

6.6.7 Step 6: Post-Processing of CFD Results

The result of the numerical calculation on the Navier-Stokes equations, according to chapter 5, are the density, the momentum and the energy in each cell center of the mesh. These results are given as input to a post-processing code developed during this research. This code give in output different kind of data:

- all the flow field data (p, T, ρ, P_0, T_0, Mach, etc..);

- the aerodynamics coefficient: C_L,C_D;

- the CFJ characteristics values: P_c, C_μ, $\dot{m_{inj}}$, $\dot{m_{suc}}$

Fig. 6.5 chain-process that start from the Gridgen and finishes to the software Tecplot used to plot all the contours and the plots for this research.

The post processing code takes in input the rstore files and gives in output the .plt files that contains the flow field data in a form that is able to be read from the software Tecplot. The code is divided in two sections:
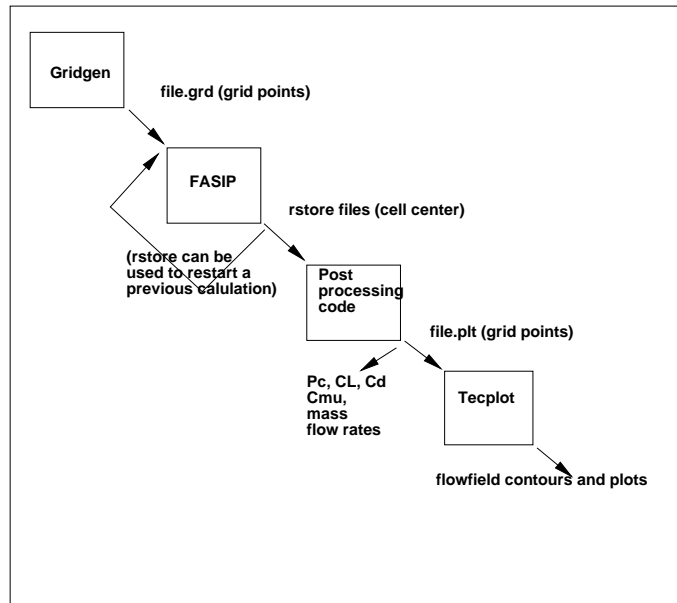
Figure 6.5: Procedure used for the numerical simulations

- the sub-routine for the calculation of C_L, C_D and C_μ;

- the sub-routine for the calculation of the mass flow rates.

The $C_L - C_D$ sub-routine code is structured as below:

- the statement of all the variables that will be used;

- the memory space allocation;

- the reading process of the rstore, init.input and datain files;

- the transformation from cell centers to grid-points;

- the computation of flow-field variables and writing of files with .plt extensions;

- the computation of C_L, C_D and C_μ

Basically, the post-processing code calculates C_L, C_D by integrating the pressure field cell by cell around the airfoil. The mass flow rate subroutine is structured in a similar way and at the end it contains also the formula for the calculation of the P_c, the V_jet (the non dimensional velocity of the jet in the case of CFJ and other parameters. When the post processing code is launched, it request to the user if the study case is a CFJ or a baseline because there are two different routine for the C_L and C_D calculation. In the case of the CFJ, for instance, the these aerodynamics coefficients should be corrected by adding them the jet reaction forces.
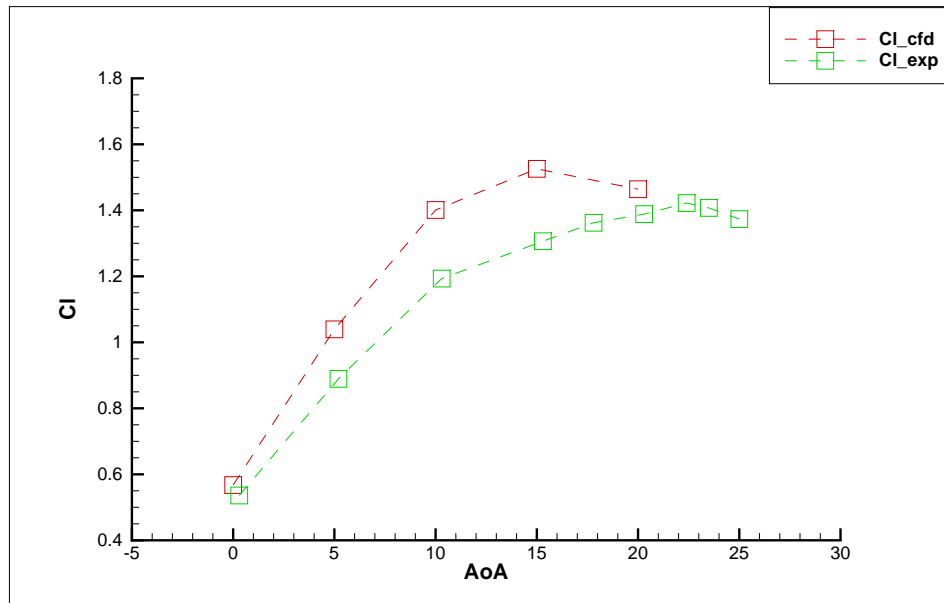
Figure 6.6: C_L for various AoA,

6.6.8 The results

For the baseline airfoil 5 AoA where chosen: $0°, 5°, 10°, 15°, 20°$ for only Mach number 0.03. The reason why were not considered others Mach number is that as showed in the formula 4.22 , both the C_L and the C_D are independent from the condition of the free stream. The experimental measurements showed on chapter 4, figure 5.13 shows a very slightly difference between the plot at different Mach number. This difference it's mostly due to the measurement error due both to the variations of the room and weather conditions and to the measurement process. The figures belows show the contours of the flow field and the aerodynamics coefficients plots.

From the baseline case, only C_L and C_D were used as results. The post processing executable calculates the pressure distribution along the surface of the airfoil for each block. The sums of each component are used to obtain the total dimensionless lift and drag for each case. Since lift is always perpendicular to the free stream flow and drag is parallel to free stream flow, the angle of attack must be included in the calculation of each coefficient. Also, the dimensionless reference length and area needs to be included to acquire the C_L and C_D per dimensionless unit length. For the baseline and the CFJ airfoil, the reference length = 1 and reference area = 2 (The chord length of 12" $(0.3048\,m)$ is normalized to 1 and the span of 24" $(0.6096\,m)$ is normalized to 2, so reference area is $1 \times 2 = 2$). Equations 6.51 and 6.52 show how the coefficients C_L and C_D can be used to obtain dimensional force values, where L and D are the lift and drag forces and S is the span area of the airfoil.

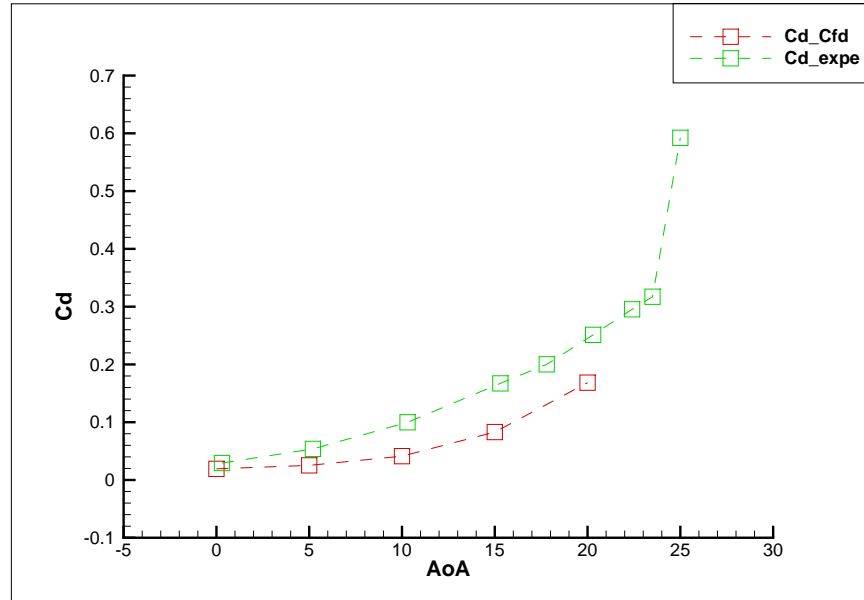$$L = C_L \cdot \frac{1}{2}\rho_\infty V_\infty^2 S \tag{6.51}$$
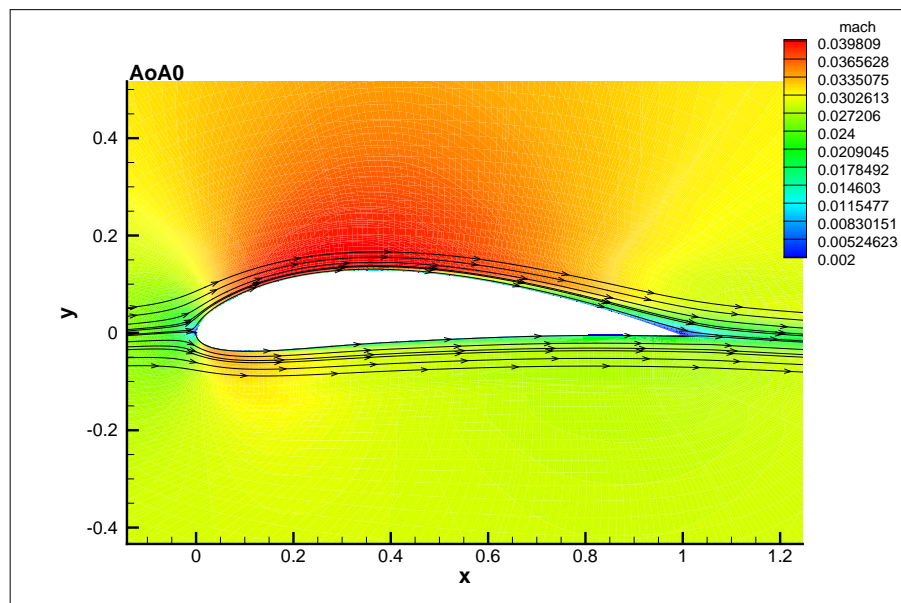
Figure 6.7: C_D for various AoA

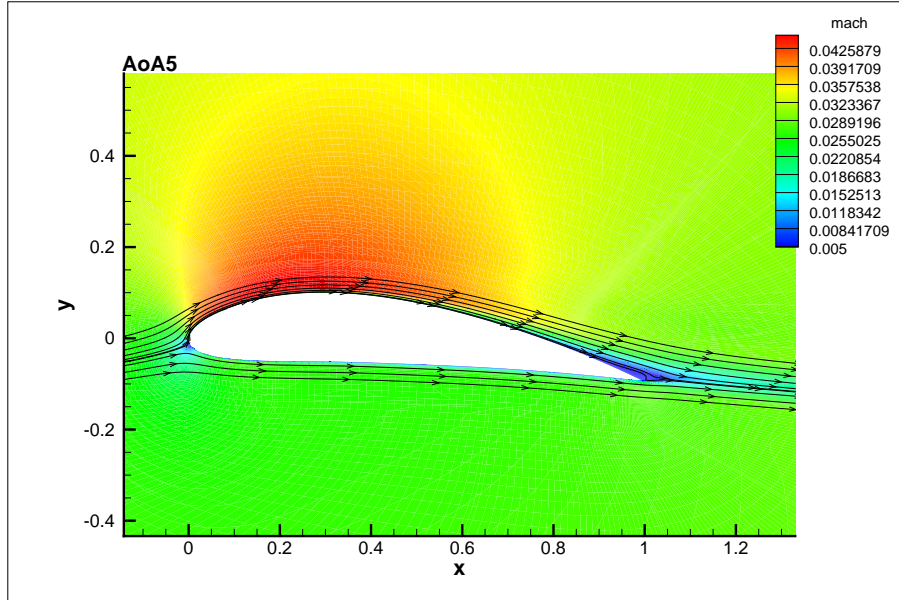

Figure 6.8: Mach number contur and streamlines, AoA 0°

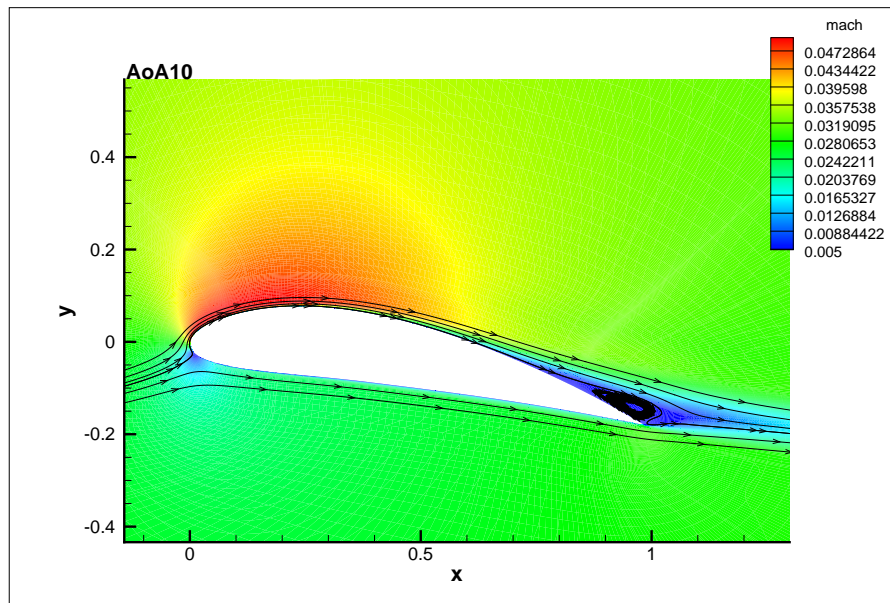Figure 6.9: Mach number contur and streamlines, AoA 5°

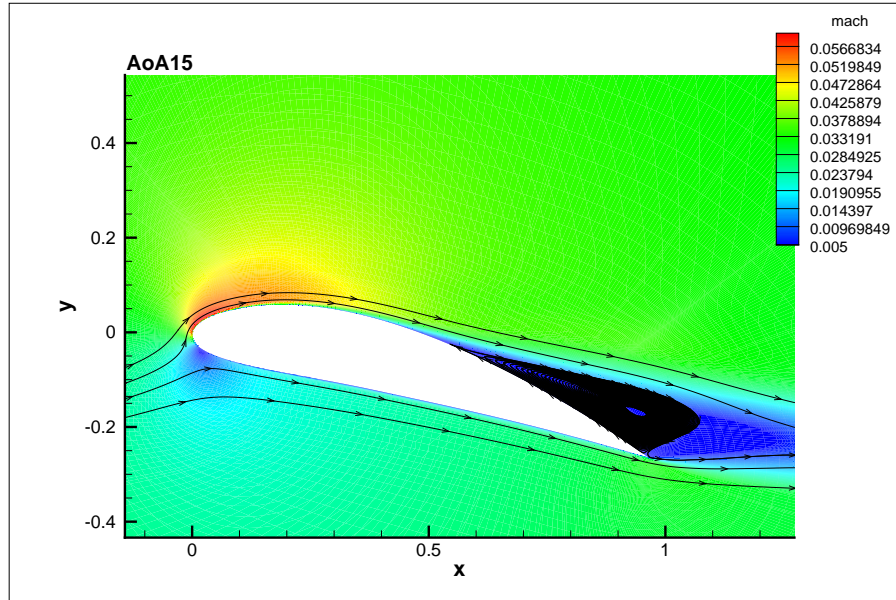Figure 6.10: Mach number contur and streamlines, AoA 10°
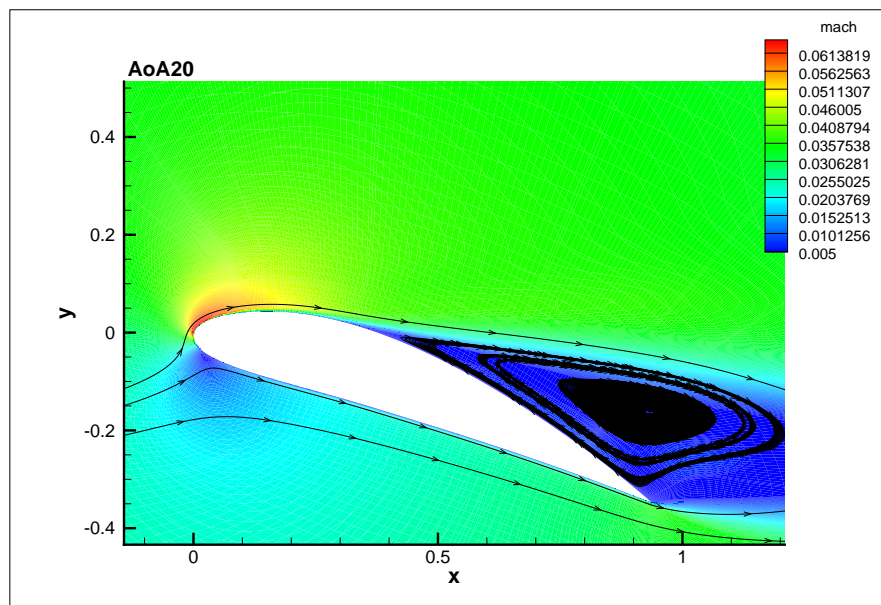
Figure 6.11: Mach number contur and streamlines, AoA 15°

Figure 6.12: Mach number contur and streamlines, AoA 20°

$$D = C_D \cdot \frac{1}{2}\rho_\infty V_\infty^2 S \tag{6.52}$$

The final values obtained for lift and drag coefficients from the baseline CFD simulations are shown in table 6.5.

α	C_L	C_D
0	.57	.0193
5	1.04	.0253
10	1.40	.0412
15	1.53	.0829
20	1.46	.1684

Table 6.5: C_L and C_D for CFD Baseline Case

6.7 The numerical investigation of the energy expenditure for a CFJ6415 airfoil profile

6.7.1 Introduction

The calculation of the energy expenditure was conducted by considering the power coefficient P_c that was introduced in the previous chapters. Like in the case of the NACA6415 baseline airfoil profile, all the study cases are 2-dimensional, because another objective of this thesis it's also to check if it's possible to obtain good numerical results by using a 2D model that in comparison with a 3D model it requests less computational resources and it gives results very fast.The numerical investigations was similar to the case of the baseline except that in the CFJ case it was necessary to re-iterate the calculation by varying the pressures in the injection and suction cavities to match the ideal C_μ and to make equals each other the injection and the suction mass flow rates.

6.7.2 The CFJ6415 mesh

The mesh of the CFJ6415 was created using the same procedure used for the baseline profile. The cad file contains the geometry of the airfoil was imported into Gridgen were the mesh was created. The CFJ airfoil geometry is more complicated respect to the baseline geometry. It was necessary to mesh the internal injection and suction cavities and the suction surface of the CFJ profile between the injection and the suction slots. Fig. 6.13, 6.14, 6.15 and 6.16 show the geometry and the final mesh of the CFJ profile and table 6.6 shows all the domains data of the CFJ airfoil.
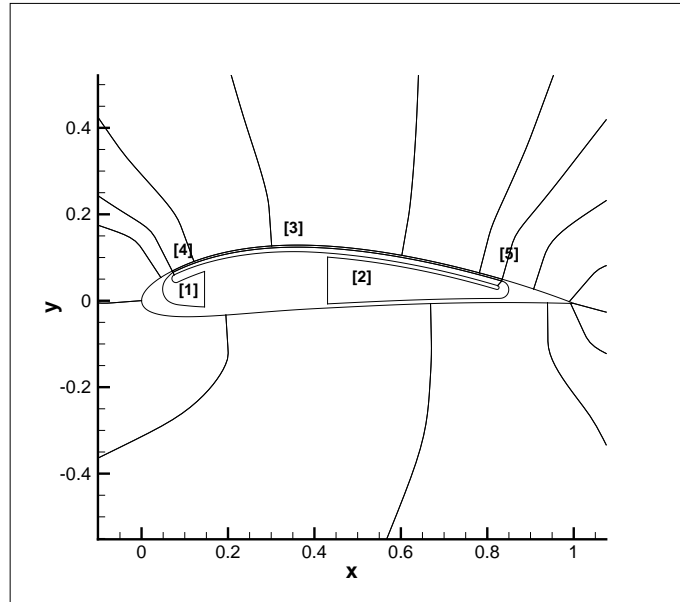
Figure 6.13: CFJ6415 airfoil profile geometry:[1]injection cavity, [2]suction cavity,[3]suction surface,[4]injection slot, [5]suction slot
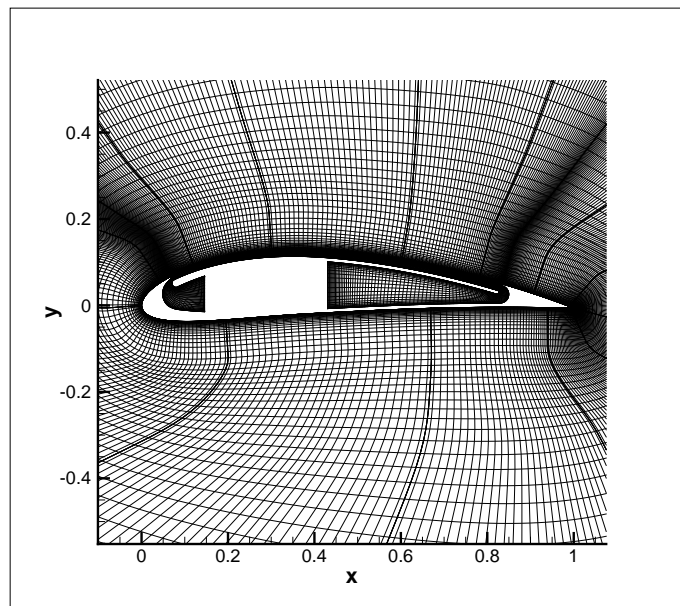

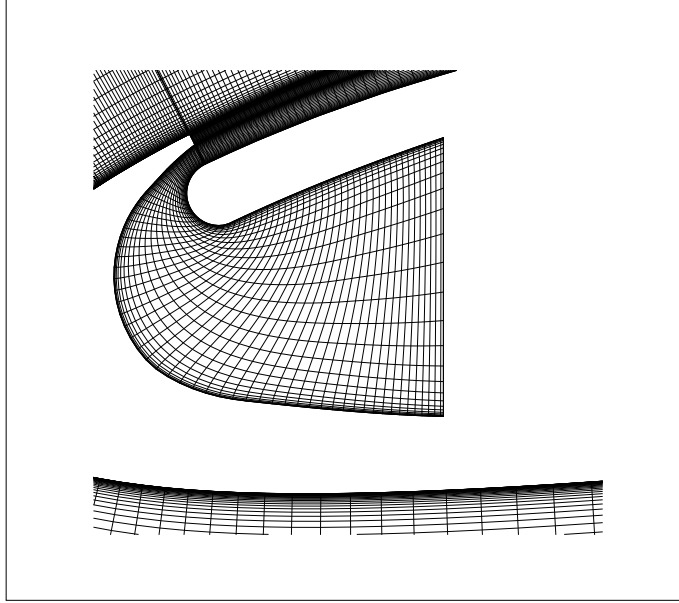Figure 6.14: CFJ6415 airfoil profile mesh

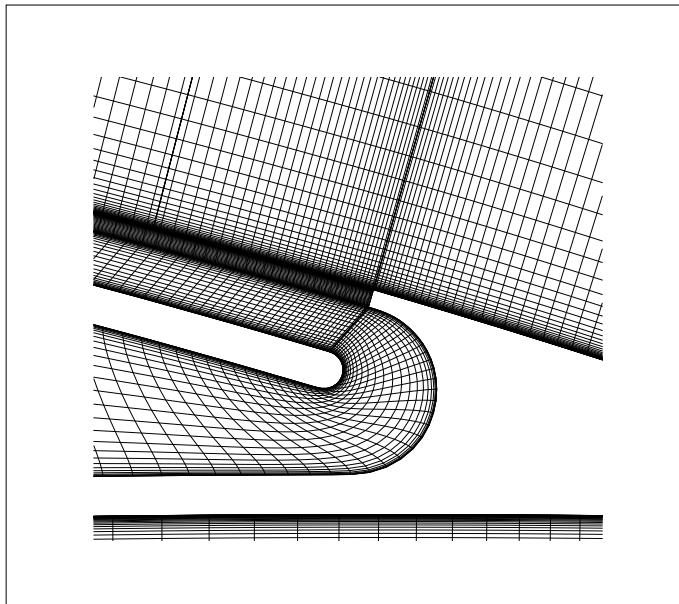Figure 6.15: CFJ6415 airfoil profile injection slot mesh

Figure 6.16: CFJ6415 airfoil profile suction slot mesh

Block	ξ-Direction	η-Direction	ζ-Direction	Total Nodes
1	61	31	0	1891
2	151	31	0	4681
3	91	31	0	2821
4	151	31	0	4681
5	31	101	0	3131
6	31	101	0	3131
7	31	101	0	3131
8	31	101	0	3131
9	31	101	0	3131
10	31	101	0	3131
11	31	101	0	3131
12	31	101	0	3131
13	31	101	0	3131
14	31	101	0	3131
15	31	101	0	3131
16	31	101	0	3131
17	31	101	0	3131
18	31	101	0	3131
19	31	101	0	3131
total	-	-	-	61039

Table 6.6: Block Allocation and dimension in term of grid points for CFJ6415 airfoil

6.7.3 Numerical investigation of Co-Flow Jet Flow Control airfoil energy expenditure

The same study cases analyzed in the experimental investigation were chosen for the numerical investigation. Like in the case of the baseline airfoil profile, the procedure below was used to launch the calculation of each study case on one of the super-computer mentioned in the previous paragraphs. Basically the procedure used is this:

- insert into init.input the experimental values of the pressure into injection and suction cavities;

- normalize the experimental pressure values and the values of the pressure variations;

- writing the appropriate boundary conditions for the CFJ airfoil in the datain;

- choosing the appropriate calculation scheme and CFL value;

The table 6.7 shows all the study cases for which the numerical investigations was made.

Mach	AoA0	AoA10	AoA20
0.04	done	done	done
0.07	done	done	done
0.1	done	done	done

Table 6.7: Study cases for the CFJ numerical investigation, with $C_\mu = 0.042$

All the study cases in tab. 6.7 are referred to $C_\mu = 0.042$ The way in which a calculation was started and the input data for a study case were similar to that used for the NACA6415 but in addition to these inputs, the CFJ airfoil simulations require some additional informations like the additional pressure and temperature conditions for the injection and suction cavities. All these data will be inserted in the `init.input`. This file contains the total pressure in the injection cavity, the temperature in the injection cavity, and the static pressure in the suction cavity. These values, like the free stream values, were found from sensor equipment in wind tunnel testing. The total and static pressures in this file are adjusted throughout the simulation to maintain equal mass flow rates exiting and entering the injection and suction cavity. Also, the C_μ can't be exactly constant and equal to 0.042, it slightly variates, and these variations are allowed into a range of 2% respect to 0.042.

For a study case, to obtain the desired results which basically means to make the mass flow rates equals, to match the desired C_μ and so to obtain the P_c, it was necessary to uses the procedure below:

- insert in the init.input the cavities pressures;

- launching the calculation;

- recording the results of the calculation on a spreadsheet;

- if the the flow rates and the C_μ are not matched modifying the pressures in the init.input and restarting the calculation;

To obtain the results very fast the first values of cavity pressures were taken from some experimental data obtained in the Wind Tunnel facility at University of Miami. These data are shown in the figures 6.17, 6.18, 6.19 and are relative to $C_\mu = 0.034$, even do this is not the desired $C_\mu = 0.042$ it's necessary to know that these data are valid because it was observed during the experimental investigation that the C_μ value measured it's not stable at all and it oscillates. The experimental data obtained are shown in tables 6.10, 6.10 and 6.10:

So for the first calculation of each study case the assumption made was that $P_{static} \simeq P_{02}$ where P_{static} is that static pressure inside the suction cavity. In the init.input we insert the total pressure into the injection cavity $P_0 1$ and the P_s in the suction cavity. For the starting point were used the values of the suction cavity total pressure showed in tab. 6.10. It was reasonable to use these values because they are almost similar to the relative static pressure values. It's necessary to say that the suction and injection sections of the pump in the wind tunnel facility are
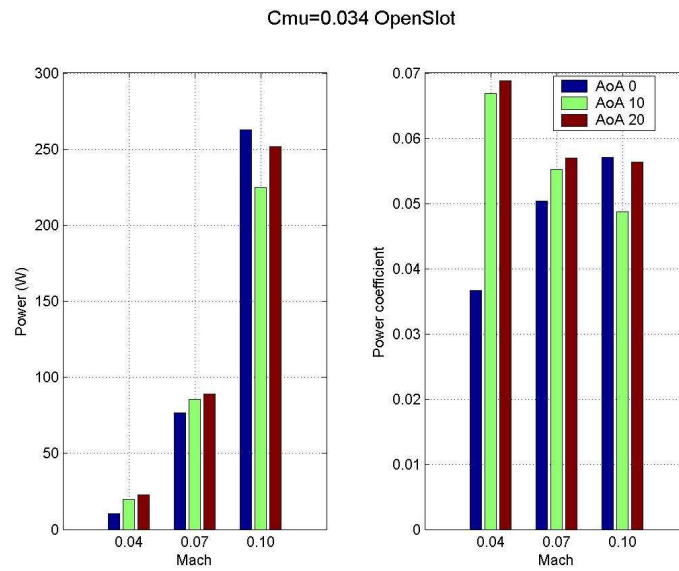
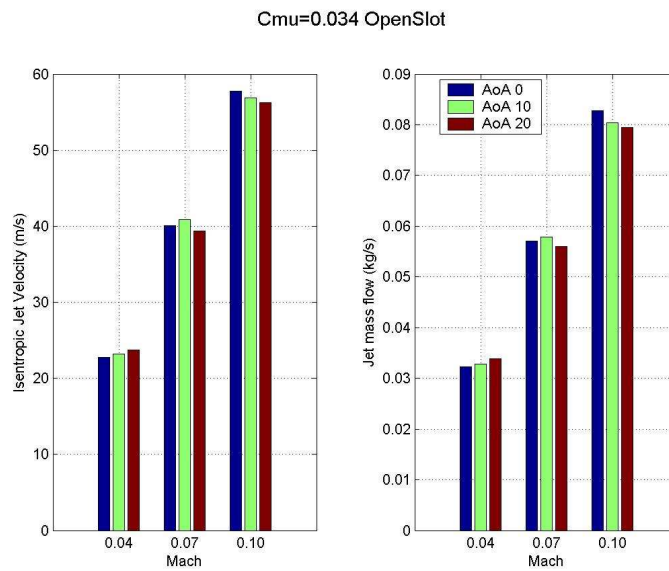Figure 6.17: CFJ6415 experimental P_c data for $C_\mu = 0.034$

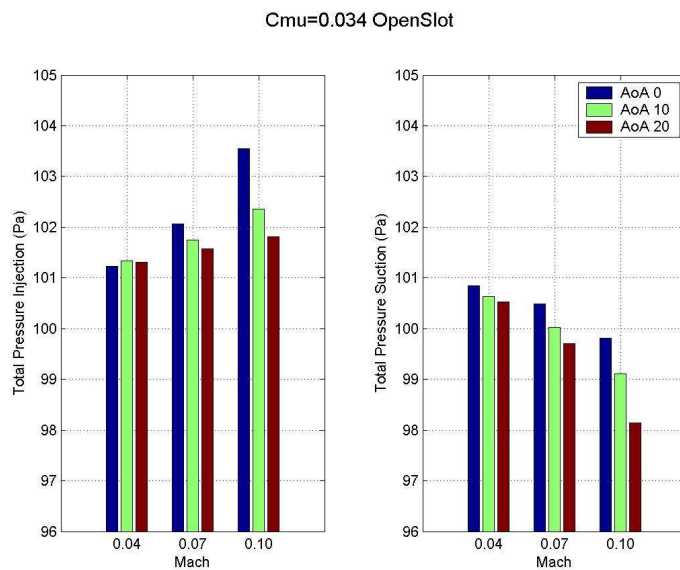Figure 6.18: CFJ6415 experimental V_{jet} data for $C_\mu = 0.034$

Figure 6.19: CFJ6415 experimental cavity pressures data for $C_\mu = 0.034$

AoA0	P_{01}(kPa)	P_{02}(kPa)
0	101.5	100.75
10	101.5	100.5
20	101.5	100.5

Table 6.8: Study cases for the CFJ numerical investigation; $Mach = 0.04$

AoA0	P_{01}(kPa)	P_{02}(kPa)
0	102.5	100.5
10	101.75	100
20	101.75	99.75

Table 6.9: Study cases for the CFJ numerical investigation; $Mach = 0.07$

AoA0	P_{01}(kPa)	P_{02}(kPa)
0	103.5	99.75
10	102.25	99
20	101.75	98

Table 6.10: Study cases for the CFJ numerical investigation; $Mach = 0.1$

placed, inside the wing, in a position that make the flows direction parallel to the wing span direction but in the CFD model of the wing the pump sections are placed in a way that the flow inside the cavities goes parallel to the chord directions. The

experimental values were normalized to be inserted into the flow by using the formula 6.18 in the subsection 5.3. are shown in the tables 6.11,6.12and 6.13.

AoA0	$\bar{P_{01}}$	$\bar{P_{02}}$
0	445.692	443.491
10	445.692	442.391
20	445.692	442.391

Table 6.11: Study cases for the CFJ numerical investigation; $Mach = 0.04$

AoA0	$\bar{P_{01}}$	$\bar{P_{02}}$
0	146.615	144.46
10	146.255	143.74
20	145.896	143.38

Table 6.12: Study cases for the CFJ numerical investigation; $Mach = 0.07$

AoA0	$\bar{P_{01}}$	$\bar{P_{02}}$
0	72.896	70.254
10	72.015	69.726
20	71.663	69.022

Table 6.13: Study cases for the CFJ numerical investigation; $Mach = 0.1$

In fig. 6.20 the meaning of the acronyms are:

- $Pt = P_{01}$ is the injection cavity total pressure;

- $Pout = P_{static} \simeq P_{02}$; P_{out} is the suction cavity static pressure;

- $\Delta C_{\mu} = \frac{C_{\mu}-0.042}{0.042}x100\%$ is the percentual variation between the C_{μ} value from the actual calculation and the ideal value of 0.042;

- $\Delta M\%$ is the percentual variation between the injection and suction flow rates respect to the injection flow rate;

For each calculation on a specific study case, the results were recorded on an Open office spreadsheet file. The actual values obtained at the end of a single calculation were analyzed, if the C_{μ} was not matched the P_{01} was modified and at once this was achieved, eventually the P_{02} was modified to match the mass flow rates keeping in mind that the suction flow rate increase as the P_{02} decreases.

NOTES	Pt	Pout	Pt – Pout	Cmu	DeltaCmu%	Minj	Msuc	DeltaM%	CL	Cd	p02 (p0ave)	Γ	Pc	CL/(CD+Pc)
1 expe	445.6920	443.4910	2.201000	0.040404	-3.800868	0.02225043840	0.03029894205	-36.172337						
2 Pt+50Pa	445.9121	443.4910	2.421095	0.046904	11.675480	0.02398203784	0.03125485521	-30.326102						
3 average	445.7500	443.4910	2.259000	0.042152	0.361574	0.02272872812	0.03060406691	-34.649272						
4 Pout+50F	445.7500	443.7111	2.038905	0.041988	-0.029291	0.02268437868	0.02856341306	-25.916665						
5	445.7500	443.9312	1.818810	0.041760	-0.572037	0.02262264535	0.02625900506	-16.073981						
6	445.7500	444.1513	1.598715	0.041487	-1.221056	0.02254860582	0.02363145769	-4.802301						
7	445.7500	444.3714		0.041116	-2.104421	0.02244743373	0.02041473489	9.055373						
8	445.7500	444.2250		0.041380	**-1.476000**	0.02251945059	0.02264085693	**-0.539118**	0.779	0.099	442.216	1.008	**0.080**	4.342

Figure 6.20: Spreadsheet for the studycase $AoA = 0$ and Mach 0.1

6.8 Results

[1]The P_c basically depends from the mass average jet velocity and jet mass flow calculated at the jet exit. The total pressure and total temperature of the injection are defined by the free stream boundary condition while the mass averaged total pressure of the suction cavity needs to be calculated using the is-entropic relation. While P_c represent the energy required at the pump, C_L and C_D data provide us with the gain in term of lift and drag. The AoA and the Mach number have influence on the P_c. All data are acquired at constant $C\mu$. The data obtainde from the CFD are presented with experimental results for comparison.

Mach contour are displayed Fig. 6.26, Fig. 6.27 and Fig. 6.28. Injection and suction cavity are displayed Fig. 6.29 and Fig. 6.30 respectively.

C_L and C_D data are presented Fig. 6.25 Experimental data show an average improvement of C_L by 13% at 0°, 19% at 10° and 18% at 20°. The augmentation obtained is mostly independent from the free stream velocity except at AoA 10° where it increases with the Mach number. Computationally, the average increase of C_L is 22% at 0°, 21% at 10° but show no increase at AoA 20° due to a stall airfoil. It's possible to see that CFD result stall earlier. This early prediction of the stall in CFD could result from the bad modelization of turbulence. Indeed the role of turbulence in energizing the boundary layer flow is foundamental to accurately predict the stall angle. At lower AoA, the lift is over predicted by around 15% for the CFJ airfoil. A similar situation characterize the baseline airfoil.

The experimental drag decrease up to 45% at M1 but no significant gain at higher Mach number. The CFD results show that the higher the Mach number the lower the drag and actually achieve 0 drag at AoA 0°. Both CFD and experimental results, for M2 and M3, shows that both of them predict a Drag that is similar to their respective baseline. However the CFD code tends to under predict the drag.

Imperfection of the surface like smoothness, tape or machining imprecision of the wing are not taken into account during the CFD simulations so this "perfect" airfoil will have increased performance with respect to the airfoil tested in the wind tunnel. This is in part an explaination of the fact that the computational C_L and C_D are different with respect to the experiments.

6.8.1 Work in Progress

More results at higher angle attack that the CFJ airfoil stalls will be presented in future works at University of Miami.
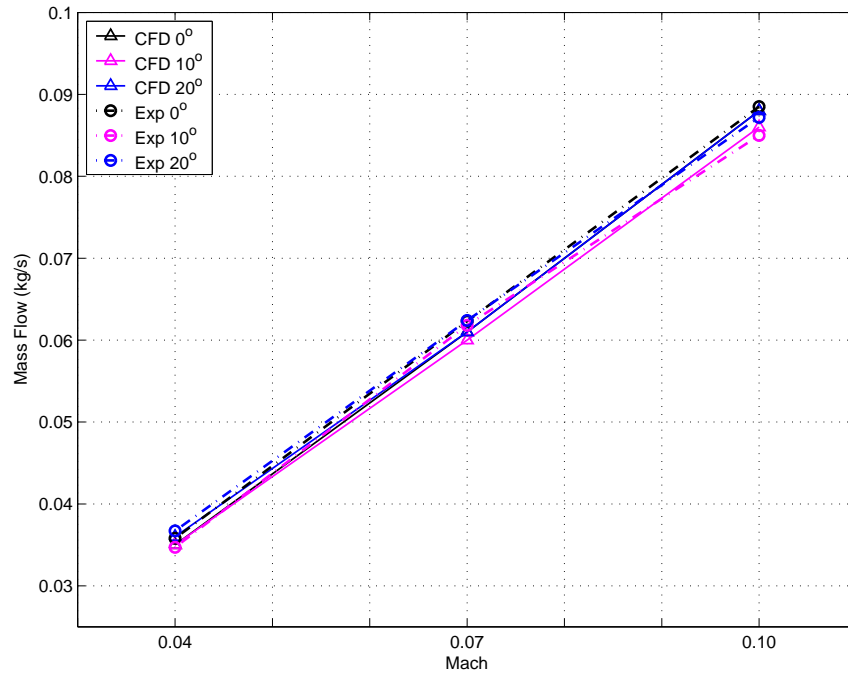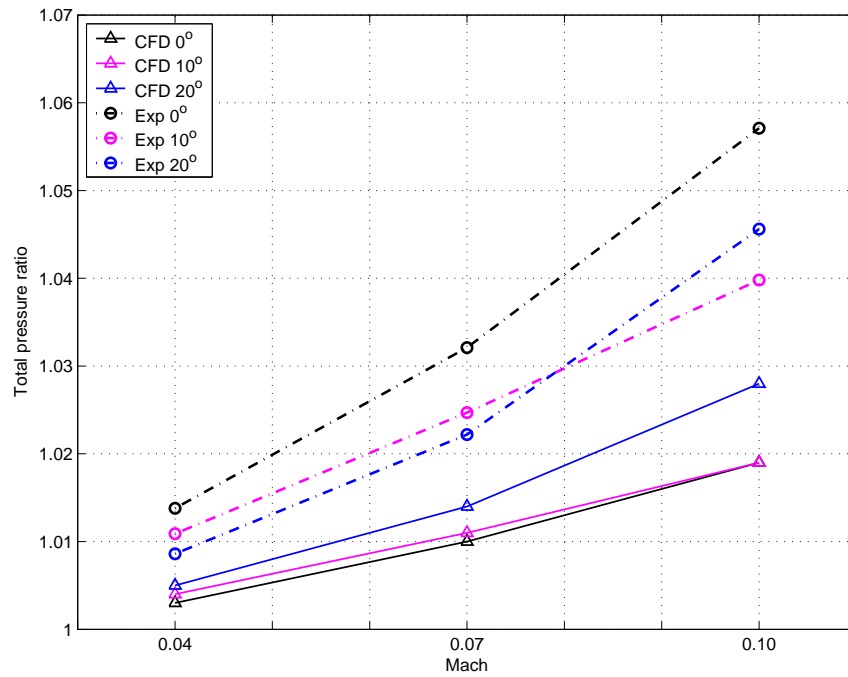
Figure 6.21: Injection mass flow rates

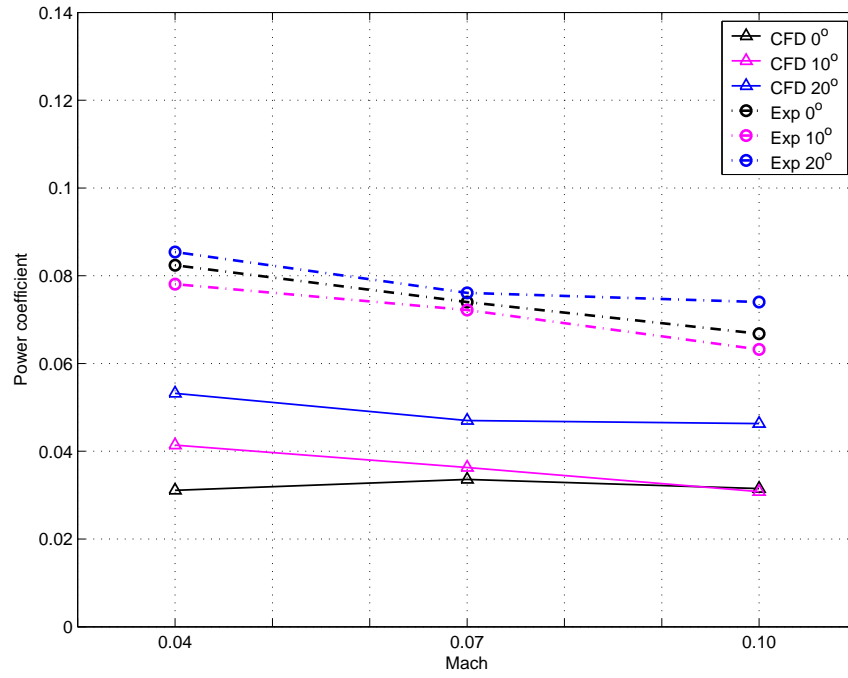Figure 6.22: Cavity total pressures ratio
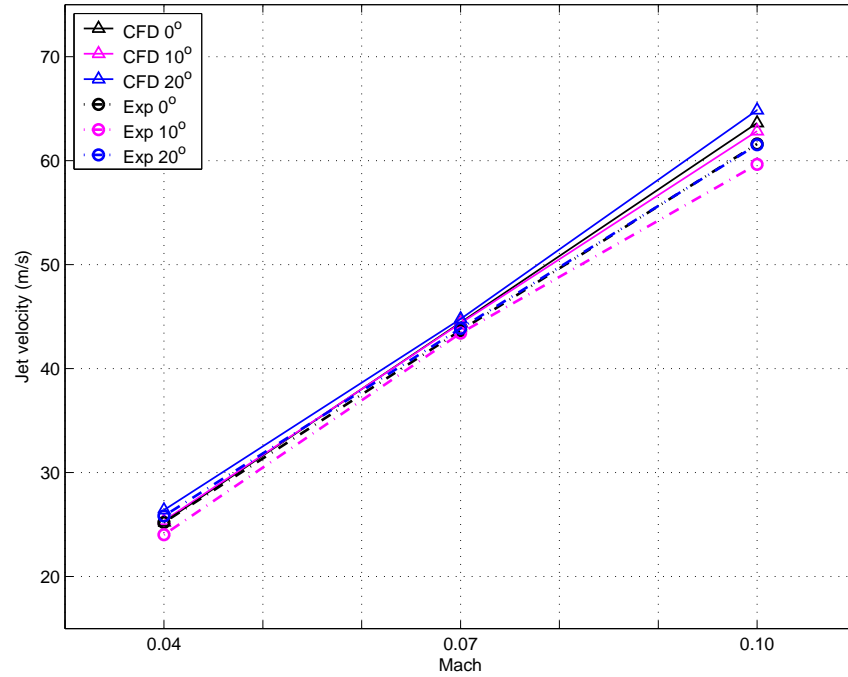
Figure 6.23: The power coefficient
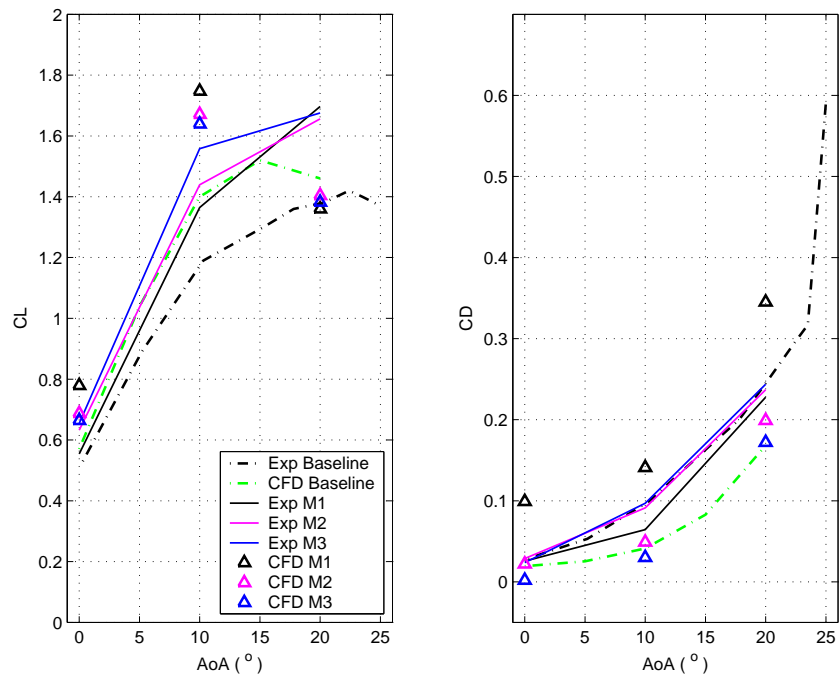

Figure 6.24: Injection jet velocity

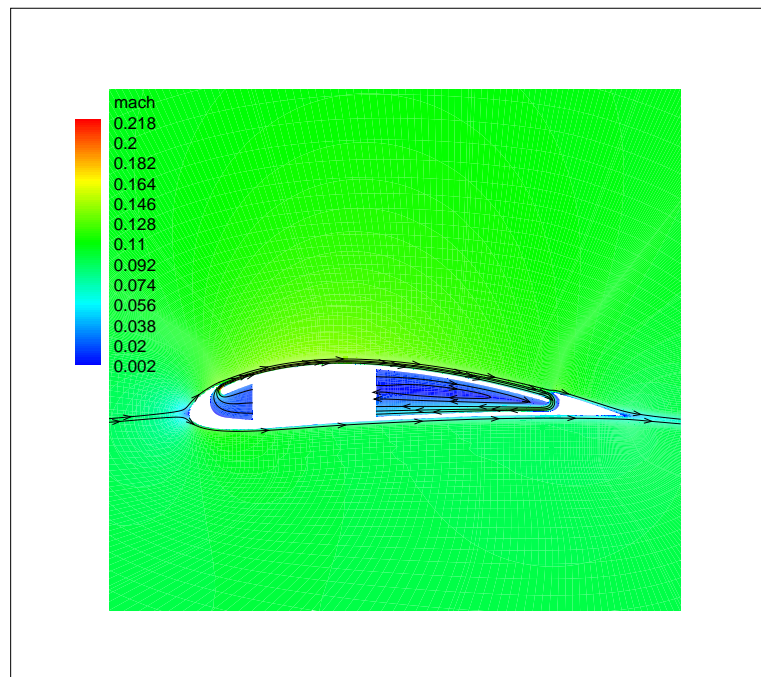Figure 6.25: Lift and Drag coefficient vs AoA
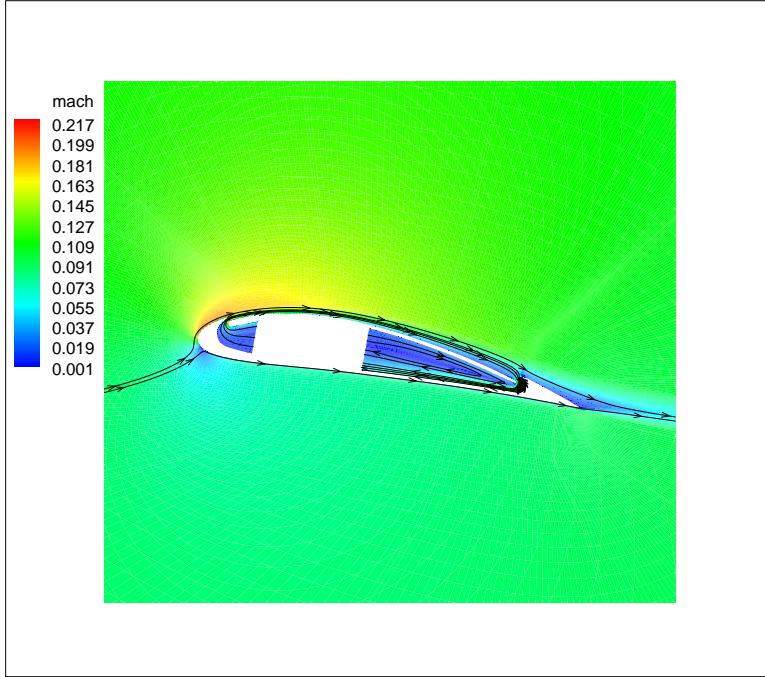

Figure 6.26: CFJ6415, Mach 0.1, A0A 0, Mach contour

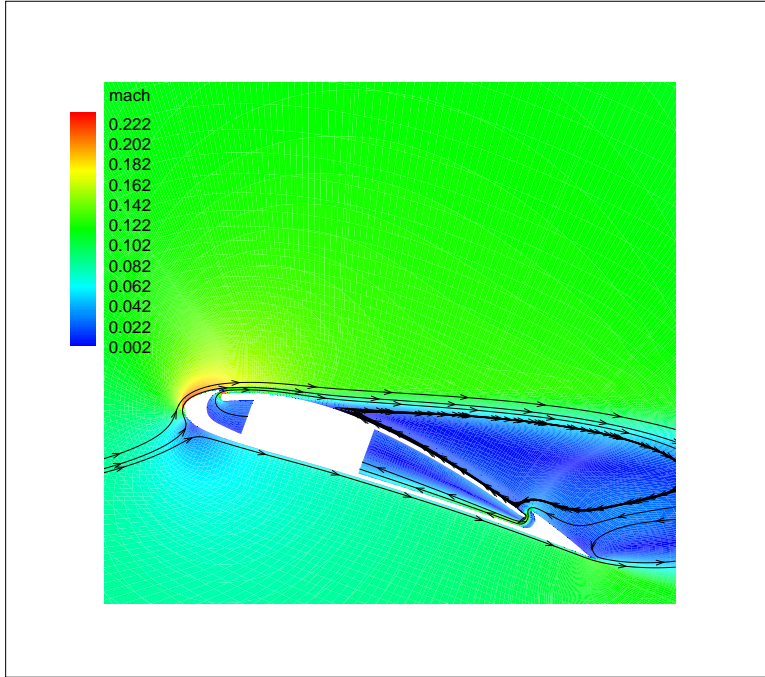Figure 6.27: CFJ6415, Mach 0.1, A0A 10, Mach contour

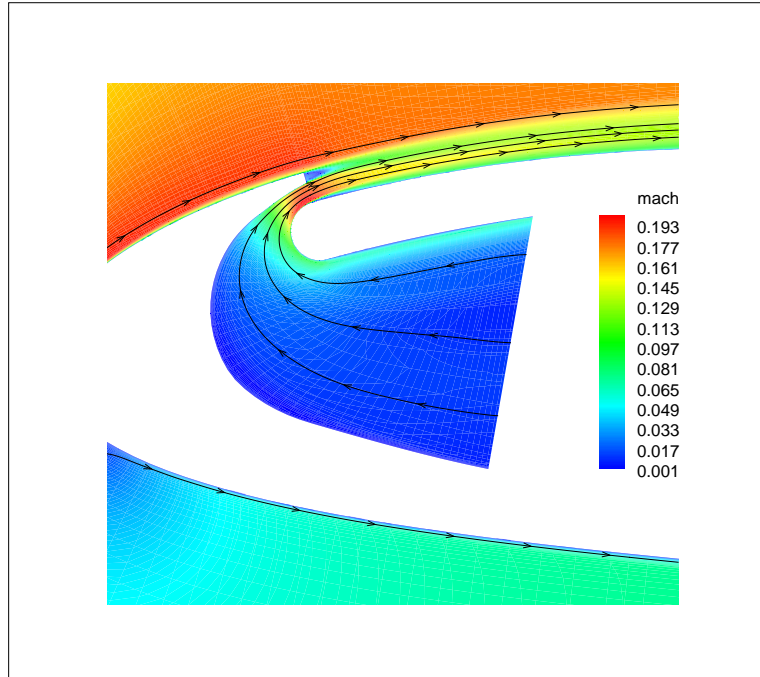Figure 6.28: CFJ6415, Mach 0.1, A0A 20, Mach contour

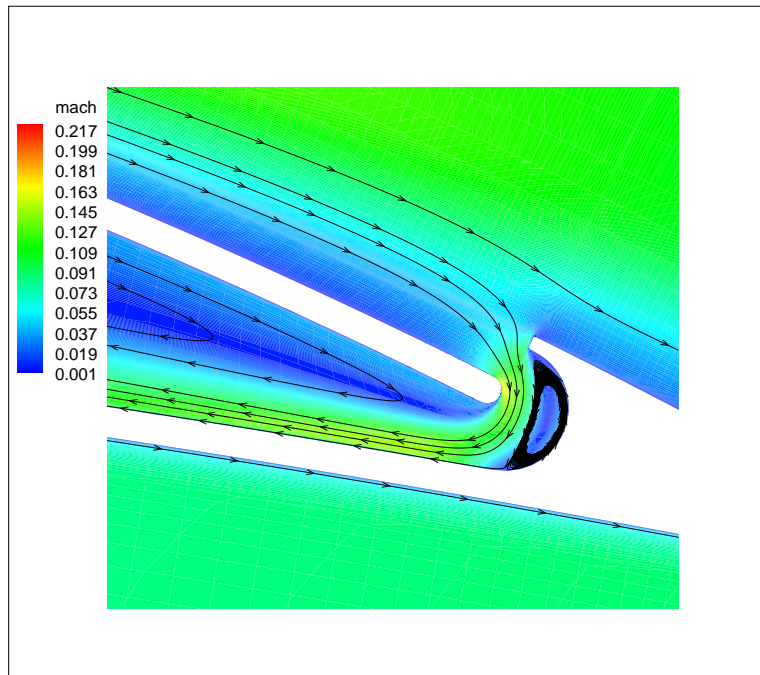Figure 6.29: CFJ6415, Mach 0.1, A0A 10,injection slot details, Mach contour

Figure 6.30: CFJ6415, Mach 0.1, A0A 10, suction slot details Mach contour

References

[1] A. Lefebvre, M. D. Fronzo, W. B. Bartow, B. Dano, and G.-C. Zha, "Experimental and Numerical Investigations of Energy Consumption for a CFJ airfoil," *AIAA Journal*, 2011.

[2] G.-C. Zha and C. Paxton, "A Novel Airfoil Circulation Augment Flow Control Method Using Co-Flow Jet." AIAA Paper 2004-2208, 2004.

[3] G.-C. Zha, C. D. Paxton, and C. A. Conley, "Effect of Injection Slot Size on the Performance of Coflow Jet Airfoil," *Journal of Aircraft*, vol. 43, pp. 987–995, 2006.

[4] G.-C. Zha and C. D. Paxton, "Novel Flow Control Method for Airfoil Performance Enhancement Using Co-Flow Jet," *Applications of Circulation Control Technologies, AIAA Book Series, Progress in Aeronautics and Astronautics*, vol. 214, pp. Chapter 10, p. 293–314, 2006.

[5] G.-C. Zha, B. F. Carroll, C. Paxton, C. A. Conley, and A. Wells, "High-Performance Airfoil Using Coflow Jet Flow Control," *AIAA Journal*, vol. 45, No. 8, pp. 2087–2090, 2007.

[6] G.-C. Zha, W. Gao, and C. D. Paxton, "Jet Effects on Coflow Jet Airfoil Performance," *AIAA Journal*, vol. 45, No. 6, pp. 1222–1231, 2007.

[7] G.-C. Zha and W. Gao, "Analysis of jet effect on co-flow jet airfoil performance with integrated propulsion system." AIAA Paper 2006-0102, 2006.

[8] G.-C. Zha, B. F. Carroll, C. Paxton, C. A. Conley, and A. Wells, "High performance airfoil using co-flow jet flow control." AIAA Paper 2005-1260, 2005.

[9] G.-C. Zha, W. Gao, and C. Paxton, "Numerical simulation of co-flow jet airfoil flows." AIAA Paper 2006-1060, 2006.

[10] W. Johnson, J. Tennant, and R. Stamps, "Leading-Edgy Rotating Cylinder for Boundery Layer Control on Lifting Surfaces ," *J. Hydronaut*, vol. 9, pp. 76–78, 1975.

[11] V. J. Modi, F. Mokhtarian, M. Fernando, and T. Yokomizo, *Moving Surface Boundary Layer Control as Applied to 2-D Airfoils*. AIAA Paper 89-0296, 1989.

[12] R. Englar and R. M. Williams, "Test Techniques for High Lift, Two Dimensional Airfoils with Boundary Layer and Circulation Control for Application to Rotary Wing Aircraft," *Canadian Aeronautics and Space Journal*, vol. 19, pp. 93–108, 1973.

[13] R. J. Englar, "Circulation Control for High Lift and Drag Generation on STOL Aircraft," *Journal of Aircraft*, vol. 12, pp. 457–463, 1975.

[14] R. J. Englar, L. A. Trobaugh, and R. Hemmersly, "STOL Potential of the Circulation Control Wing for High-Performance Aircraft," *Journal of Aircraft*, vol. 14, pp. 175–181, 1978.

[15] R. J. Englar, "Circulation Control Pneumatic Aerodynamics: Blown Force and Moment Augmentation and Modifications; Past, Present and Future." AIAA 2000-2541, June 2000.

[16] Y. Liu, L. N. Sankar, R. J. Englar, K. K. Ahuja, and R. Gaeta, "Computational Evaluation of the Steady and Pulsed Jet Effects on the Performance of a Circulation Control Wing Section." AIAA Paper 2004-0056, 42nd AIAA Aerospace Sciences Meeting and Exhibit, Reno, Nevada 5 - 8 Jan 2004.

[17] G.-C. Zha, W. Gao, and C. Paxton, "Jet Effects on Co-Flow Jet Airfoil Performance," *AIAA Journal, No. 6,*, vol. 45, pp. 1222–1231, 2007.

[18] G. S. Jones, "Pneumatic Flap Performance for a 2D Circulation Control Airfoil, Stedy & Pulsed." *Applications of Circulation Control Technologies*, Chapter 7, p. 191-244, Vol. 214, Progress in Astronautics and Aeronautics, AIAA Book Series, Editors: Joslin, R. D. and Jones, G. S., 2006.

[19] A. Glezer and M. Amitay, "Synthetic Jets," *Annual Review of Fluid Mechanics*, vol. 24, 2002.

[20] R. Holman, Y. Utturkar, R. Mittal, and L. Cattafesta, "Formation Criterion for Synthetic Jets," *AIAA Journal*, vol. 43, No. 10, pp. 2110–2116, 2005.

[21] T. C. Corke and M. L. Post, " Overview of Plasma Flow Control: Concepts, Optimization, and Applications." AIAA Paper 2005-0563, Jan. 2005.

[22] C. Enloe, T. E. McLaughlin, G. I. Font, and J. W. Baughn, " Frequency Effects on the Efficiency of Aerodynamic Plasma Actuator ." AIAA Paper 2006-0166, Jan. 2006.

[23] G.-C. Zha and D. C. Paxton, "A Novel Flow Control Method for Airfoil Performance Enhancement Using Co-Flow Jet." *Applications of Circulation Control Technologies*, Chapter 10, p. 293-314, Vol. 214, Progress in Astronautics and Aeronautics, AIAA Book Series, Editors: Joslin, R. D. and Jones, G.S., 2006.

[24] G.-C. Zha, C. Paxton, A. Conley, A. Wells, and B. Carroll, "Effect of Injection Slot Size on High Performance Co-Flow Jet Airfoil," *AIAA Journal of Aircraft*, vol. 43, 2006.

[25] G.-C. Zha, B. Carroll, C. Paxton, A. Conley, and A. Wells, "High Performance Airfoil with Co-Flow Jet Flow Control," *AIAA Journal*, vol. 45, 2007.

[26] Wang, B.-Y. and Haddoukessouni, B. and Levy, J. and Zha, G.-C., "Numerical Investigations of Injection Slot Size Effect on the Performance of Co-Flow Jet Airfoil," *Journal of Aircraft*, To appear 2008.

[27] B. P. E. Dano, D. Kirk, and G.-C. Zha, "Experimental Investigation of Jet Mixing Mechanism of Co- Flow Jet Airfoil." AIAA-2010-4421, 5th AIAA Flow Control Conference, Chicago, IL, 28 Jun - 1 Jul 2010.

[28] B. P. E. Dano, G.-C. Zha, and M. Castillo, "Experimental Study of Co-Flow Jet Airfoil Performance Enhancement Using Micro Discreet Jets." AIAA Paper 2011-0941, 49th AIAA Aerospace Sciences Meeting, Orlando, FL, 4-7 January 2011.

[29] Y.-Q. Shen and G.-C. Zha, "Improvement of the WENO Scheme Smoothness Estimator," *International Journal for Numerical Methods in Fluids*, 2009.

[30] Y.-Q. Shen, G.-C. Zha, and B.-Y. Wang, "Improvement of Stability and Accuracy of Implicit WENO Scheme," *AIAA Journal*, vol. 47 No. 2, pp. 331–344, 2009.

[31] B.-Y. Wang and G.-C. Zha, "A General Sub-Domain Boundary Mapping Procedure For Structured Grid CFD Parallel Computation," *AIAA Journal of Aerospace Computing, Information, and Communication*, vol. 5 No. 11, pp. 425–447, 2008.

[32] X. Chen and G.-C. Zha, "Implicit Application of Non-Reflective Boundary Conditions for Navier-Stokes Equations in Generalized Coordinates," *International Journal for Numerical Methods in Fluids*, vol. 50 No. 7, pp. 767–793, 2006.

[33] X. Chen and G.-C. Zha, "Fully Coupled Fluid-Structural Interactions Using an Efficient High Solution Upwind Scheme," *Journal of Fluid and Structure*, vol. 20 No. 8, pp. 1105–1125, 2005.

[34] X. Chen and G.-C. Zha, "Fully Coupled Fluid-Structural Interactions Using an Efficient High Solution Upwind Scheme," *Journal of Fluid and Structure*, vol. 20 No. 8, pp. 1105–1125, 2005.

[35] G.-C. Zha, "A Low Diffusion Efficient Upwind Scheme," *AIAA Journal*, vol. Vol.43, No.5, pp. 1137–1140, 2005.

[36] Z. Hu and G.-C. Zha, "Calculations of 3D Compressible Using an Efficient Low Diffusion Upwind Scheme," *International Journal for Numerical Methods in Fluids*, vol. Vol.47, pp. 253–269, 2004.

[37] G.-C. Zha, "Boundary Layer Loss Mechanism and Justification of Wall Functions for Turbulence Modeling," *AIAA Journal*, vol. Vol.42 No. 11, pp. 2387–2390, 2004.

[38] Y. Shen and G.-C. Zha, "Simulation of flows at all speeds with high- order weno schemes and preconditioning." AIAA Paper 2009-1312, 2009.

[39] Y. Shen and G.-C. Zha, "High order finite differencing schemes and their accuracy for cfd." AIAA Paper 2009-1137, 2009.

[40] B. Wang and G.-C. Zha, "Comparison of a low diffusion e-cusp and the roe scheme for rans calculation." AIAA Paper 2008-0596, 2008.

[41] B.-Y. Wang, B. Haddoukessouni, J. Levy, and G.-C. Zha, "Numerical Investigations of Injection Slot Size Effect on the Performance of Co-Flow Jet Airfoil," *AIAA Journal of Aircraft*, vol. Vol.45 No. 6, pp. 2084–2091, 2008.

[42] A. J. Wells, "Experimental Investigation of An Airfoil with Co-Flow Jet Flow Control," Master's thesis, University of Florida, 2005.

[43] D. Kirk, *Experimental and numerical investigation of an high performance co-flow jet airfoil.* 2009.

[44] I. H. Abbott and A. E. V. Doenhoff, *Theory of Wing Sections.* Dover Publications, Inc., 1959.

[45] J. Aguirre, "Study of 3-dimensional co-flow jet airplane and high-rise building flow using cfd simulation," Master's thesis, University of Miami, 2008.

[46] G.-C. Zha, "Computational fluid dynamics class notes." MEN 614, Department of Mechanical and Aerospace Engineering, University of Miami, Spring 2007.

[47] K. A. Hoffmann and S. T. Chiang, *Computational Fluid Dynamics Volume 1, 4th Edition.* Engineering Education System, 2004.